Design and Control of A Minimally Constrained Cobot for Improving Bone Cuts in Total Knee Arthroplasty

by

Richard Emrich

B.Sc. (Eng.), University of Guelph, 1997

A thesis submitted in partial requirement
of the requirements for the degree of:

Master of Applied Science

in

The Faculty of Graduate Studies
(Mechanical Engineering)

We accept this thesis as conforming
to the required standard:

The University of British Columbia

March, 2000

Department of Mechanical Engineering

The University of British Columbia
Vancouver, Canada

Date April 25th, 2000

Abstract

Total knee arthroplasty (TKA) requires accurate placement of the prosthetic components to avoid premature failure, and traumatic revision surgery. Accuracy of frontal plane alignment is particularly crucial in ensuring maximized prosthesis longevity. Increasing the accuracy of bone cuts would decrease the need for revision surgery.

Errors introduced by radiographic technique, radiographic measurements, and alignment jigs can be reduced by improving frontal plane alignment calculations. A key location necessary for this calculation is the centre of the knee. A point probe could be used to digitize the surface of the knee, which would allow for an accurate calculation of a centre point. This method is susceptible to imperfections in the surface of the knee, which are commonplace in TKA. A "v" probe and flat probe design are presented, and are shown in simulations to be more robust in locating the centre of rounded anatomical features, such as the condyles of the knee.

Implementation errors are also major contributors to inaccurate frontal plane alignment. Increasing this accuracy may be possible by harnessing the accuracy of robots. Actively powered robots have failed to be widely accepted in surgical applications because of safety concerns. Collaborative robots, or cobots, reduce these safety concerns by being completely passive. Under computer control, cobots only constrain the user's motions by orienting frictional constraints.

A parallel architecture would be desirable for TKA because of it's stiffness. The key component for the cobot is a continuously variable transmission (CVT), but no CVT is currently suitable for use with the parallel manipulator. To address this, a linear CVT was created, and is discussed with respect to its benefits, limitations, and areas requiring future work.

The concept of a minimally constrained cobot is also introduced. This type of cobot is particularly well suited to guiding objects to areas with dimensionality greater than one. This makes them well suited to TKA, where the object is to orient a three dimensional cutting plane to guide the bone saw. A control strategy for controlling minimally constrained cobots is presented, along a 3 dimensional simulation of results.

The major contribution of this thesis is the development of a framework for minimally constrained parallel cobots for TKA. Future work will be focused on the design, construction and controller implementation of a 6 DOF cobot prototype.

Table of Contents

List of Figures

Acknowledgements

Many thanks go to my wife, Melanie DeHaan for being especially supportive of my work over the last few years. I would also like to thank my supervisor, Antony Hodgson, for spending so much time and effort making this a successful venture; Dr. Robert McGraw for his insight into TKA surgery which made defining the problem so much easier; and the Canadian Natural Sciences and Engineering Research Council and Johnson & Johnson Canada, Inc., who contributed to an NSERC Industrial Postgraduate Fellowship.

Preface

Chapter 2 of this thesis was previously published as a conference paper:

> Inkpen K, Emrich R and Hodgson AJ. Probe design to robustly locate anatomical features. In *Lecture Notes in Computer Science (Vol. 1496): Medical Image Computing and Computer-Assisted Intervention*, pp. 335-342, Springer-Verlag, Proceedings of MICCAI '98, Cambridge, MA, October 1998.

As the second author, I collaborated with a fellow student, Kevin Inkpen, and my supervisor, Dr. Antony Hodgson, on the simulations described in the paper. Kevin and I co-wrote the paper and our contributions were substantially equal.

Chapter 3 of this thesis has been submitted as a conference paper:

> Emrich R and Hodgson AJ. A continuously variable transmission element for a parallel cobot. *IMECE 9th Annual Symposium on Haptic Interfaces for Virtual Environment and Teleoperator Systems*, to be held in Orlando, FL, November 2000; submitted February 15, 2000.

As the first author on this paper, I developed the concept described therein in collaboration with my supervisor, Dr. Antony Hodgson, developed the analysis, designed and built the mechanism and wrote the paper (with editorial suggestions from my supervisor and co-author).

Confirmation:

I agree that the contributions of the author are as stated above.

Apr 25, 2000

Date

Dr. Antony J. Hodgson
Department of Mechanical Engineering
University of British Columbia

Chapter 1 – Introduction and Background

1.0 Total Knee Arthroplasty (TKA)

1.1 Need for TKA

Pathological conditions of the knee include osteoarthritis, rheumatoid arthritis and general trauma of the joint. These conditions lead to painful degradation of the knee joint, causing a decrease in life quality. Knee arthroplasty involves invasive resurfacing of the knee joint, and is one method used to correct pathological conditions of the knee.

Osteoarthritis is present in about 68% of all TKAs performed and is an activity related disease (Rand 1991). Alignment, such as bow-leggedness, and loading contribute to the onset and progression of osteoarthritis (Chao 1995). In the end, the primary indication for TKA is pain (Rathjen 1998). A computer generated example of an osteoarthritic knee, and subsequent resurfacing of the knee joint is shown in Figure 1.

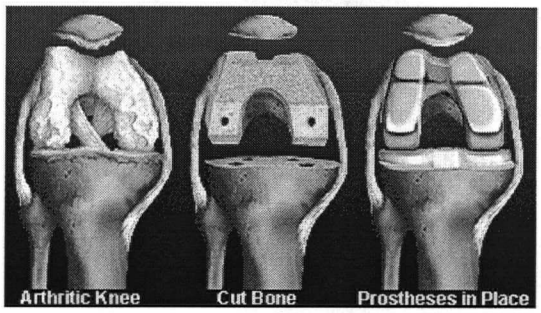

Figure 1. Replacement of an Arthritic Knee Surface (Source Unknown)

1.2 Surgical Action

Primary total knee arthroplasty (TKA) is performed roughly 150 000 times a year in the United States (Rathjen 1998). It involves removing the articular surfaces of the distal femur, proximal tibia and posterior patella, and replacement with metal and ultra high molecular weight polyethylene (UHMWPE) prostheses. The cutting and resurfacing of the bones substantially reduces the knee pain.

1.3 Purpose of TKA

Maximizing the lifespan of the prostheses is achieved in part by reproducing normal alignment of the lower limb. The aim is to reduce stresses on any one part of the knee joint, having a three fold effect:

1. Restoration of normal function and kinematics of the knee
2. Reduction in pain. Pain is often due to unequal distribution of stresses on the knee joint and surrounding soft tissue structures
3. Improved lifespan of the knee prosthesis

1.4 Prosthesis Longevity

Although TKA surgery vastly improves the quality of life of a patient, the implanted components have a finite lifespan. Once the prosthesis fails, revision surgery must take place, which involves removing and replacing the components. Both the conditions accompanying aseptic loosening (osteolysis) and the drilling and cutting needed in revision surgery are traumatic to the patient. In the next section, we look at risk factors contributing to component failure in an attempt to understand the scope of possible improvements.

1.4.1 Longevity Indicators

In 1991, a study by Rand and Ilstrup discussed factors affecting prostheses survivorship. They identified five factors that gave the best component lifespan in TKA (Rand 1991). They are: diagnoses of rheumatoid arthritis, having primary TKA, being sixty years or older, using a condylar prosthesis with a metal backed tibial component and being female. Overall, the success rate was 97 % over 10 years for those with all factors present and 81% for the entire 9200 TKAs performed. An illustration from the study is included in Figure 2.

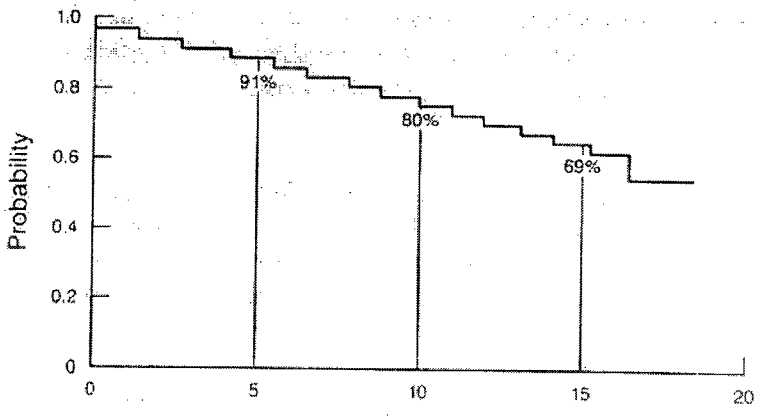

Figure 2. Survivorship Graph for TKA at 15 Years

(from Rand et al, J Bone Joint Surg [Am] 73:397, 1991.)

Interestingly, the same study found that neither cementing versus cementless prostheses nor saving the posterior cruciate ligament versus sacrificing had any significant effect on the outcome. This result was corroborated by another study (Pereira 1998).

1.4.2 Frontal Plane Alignment and Longevity

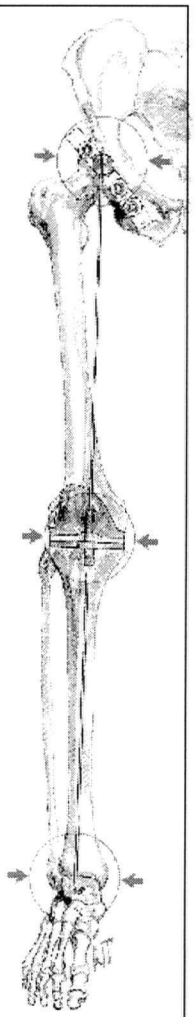

Figure 3 - Mechanical Axis of Lower Limb (Courtesy of Johnson and Johnson)

Background of Alignment Angles

A primary method of assessing lower limb alignment involves the notion of a mechanical axis (Krackow 1990). The mechanical axis of the femur is a line from the femoral head to the knee centre, and the mechanical axis of the tibia is a line from the knee centre to the ankle centre (see Figure 3). The ankle is taken at the midpoint of the inner edges of the malleoli and one half the height of the talus (Kim 1993). Normal alignment is achieved when the mechanical axis of the tibia and femur are colinear in the frontal plane (Chao 1994). The mechanical tibiofemoral angle is the angle between the two axes in the frontal plane with positive values representing varus.

The anatomic axis of the tibia and femur is a best fit line representing the shaft of the bone. The anatomic tibiofemoral angle is the frontal plane angle between these axes and is reported to be about 7°. The anatomic axis is more dependent on the individual and has less biomechanical significance than the mechanical tibiofemoral angle (Chao 1994). Many older survivorship studies quote this angle.

The second condition, which must be considered, is the establishment of a proper joint line (Krackow 1990). The joint line is roughly horizontal and represents the contact surfaces of the knee joint in full extension (Kim 1993). Excessive tilting of this line is related to failure through increases in shear forces across the joint (Chao 1994). Severe tilting also contributes to osteoarthritis over time, even with correct axial alignment (Chao 1994). This joint line can take an infinite number of orientations without affecting the normal lower limb mechanical axis. There are two basic ways of defining proper joint lines (Krackow 1990).

Classical alignment dictates that the joint line fall perpendicular to the mechanical axis of the limb. The femur has a valgus cut equal to the tibiofemoral angle. The tibia is therefore cut on a plane perpendicular to its mechanical axis. Anatomic alignment is less popular and dictates that the joint line be parallel to the ground (Krackow 1990).

Studies, such as Bargren et al., show postoperative varus knees have very poor outcomes (Bargren 1983). Varus knees leave the ground reaction force passing further medially than the normal knee, which increases moments experienced about the joint. Many surgeons try to err on the side of valgus to be safe.

Tolerance of Frontal Plane Misalignment

Poor frontal plane alignment has been identified as a contributing factor to component failure by encouraging loosening of the components, component fracture and instability of the knee (Moreland 1988; Figgie 1989; Rand 1991). Research by Jeffrey et al. found that misalignment in the frontal plane by more than 3° resulted in an increase in loosening of 21% over knees misaligned by less than 3° (Jeffery 1991). Rand reports that ensuring accurate frontal plane alignment reduces the need for revision surgery (Rand 1991). It is generally accepted that frontal plane misalignment of less than 2 degrees produces acceptable outcomes (Reed 1997), however no studies have sufficient precision to make conclusions about greater accuracy requirements.

Since surgical technique heavily influences frontal plane alignment, this can be seen as a place where substantial improvements could be made.

Surgical Accuracy

Inkpen reports a meta-analysis of postoperative TKA alignment studies (Inkpen K.B. 1999). The overall alignment standard deviation was 2.57°. This was based on 7 studies that reported alignment for a total of 753 postoperative knees. The standard deviation on femoral bone cuts was 1.93°. This figure was based on 5 studies reporting 540 knees. Lastly, the standard deviation on tibial bone cuts was 1.86°. 8 studies contributed a total of

1072 knees to the tibial meta-analysis. Inkpen takes care to mention that these numbers represent a conservative estimate of alignment accuracy, since the best surgeons are often chosen to participate in studies.

Sources of Error in Frontal Plane Alignment

The most common methods of achieving axial alignment in primary TKA are cutting jigs. They construct a cutting surface coplanar with the intended cut. There are two main methods of placing this cutting surface; using a reference rod placed inside the bone and using external anatomical structures. Each of these methods has advantages and disadvantages, and they are both still used.

In both cases, the surgeon is responsible for determining the height and angle of the resection from radiographs of the bones. This step is susceptible to measurement errors and implementation errors caused by improper seating of the saw blade.(Lennox 1988)

Extramedullary Alignment Jigs

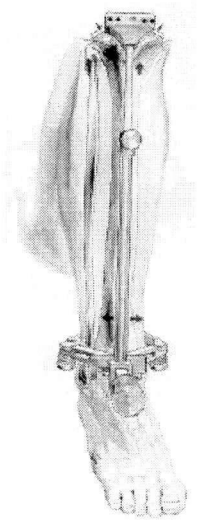

Figure 4. Extramedullary Tibial Rod (Courtesy of Johnson and Johnson)

Extramedullary alignment jigs exploit the external anatomical landmarks to place the cutting guide. On the femoral cut, one end of the alignment jig is anchored to the condyles and the other end approximates the location of the femoral head (see Figure 4). In a tibial cut, a clamp on the ankle approximates the ankle centre. Approximation error is inevitable with extramedullary jigs.

Intramedullary Alignment Jigs

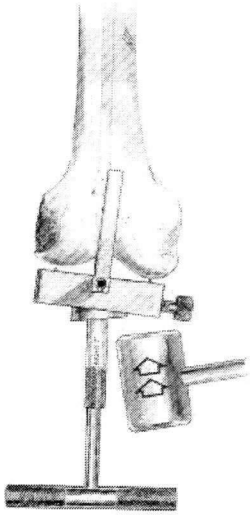

Figure 5. Intramedullary Femoral Rod (Courtesy of Johnson and Johnson)

Intramedullary alignment jigs employ a rod inserted into the medullary canal of the bone (see Figure 5). The rod gives a reference axis to relate cutting angles from the radiograph to placement of the cutting guide. Difficulties with rod placement are encountered since the rod must pass through the middle of the bone for best results. Reed et al. showed that the notch used to indicate the centre of the knee is 7mm medial to the correct rod insertion point.

Intramedullary rods were shown to improve the accuracy and reproducibility of the bone cuts in the femoral case over extramedullary alignment (Cates 1993; Jessup 1997; Teter 1995b). Most of the research indicates that tibial bowing is present in enough cases to be unreliable on the tibia (Cates 1993; Dennis 1993; Jessup 1997; Simmons 1991; Teter 1995b), and at best the differences were insignificant (Dennis 1993; Evans 1995; Ishii 1995). Intramedullary alignment is not appropriate for excess femoral bowing either (Jiang 1989; Moreland 1991; Teter 1995a).

Errors in Assessing Axial Alignment

The alignment of the lower limb depends on the location of the knee with respect to both the femoral head and the ankle. Accurate determination of these relationships requires long standing radiographs (Jessup 1997; Petersen 1988). Short film radiographs cannot accurately determine the alignment because extrapolation of the location of anatomy occurs. This is important, since survivorship studies can use short radiographs to determine accuracy of implementation. In other cases, the research may not even include explicit mention of the types of radiographs used.

Another problem is that of perspective error. Proper alignment is defined in the frontal plane, but there is no guarantee that when a radiograph is made, it is of the true frontal plane (Green 1994). On long standing radiographs, the extremes of the radiograph are distorted as the x-rays hit the film at more acute angles. The length of the bone is not accurately reproduced on the radiograph and therefore cannot be used for accurate locating of anatomy. The radiograph are also subject to changes in the distance between the patient, the camera and the x-ray sensitive film.

If current radiographic techniques continue to be used to determine bone resection angles, standardisation of patient stance is necessary (Chao 1994; Cooke 1991; Cooke 1987). Compensation methods for limb rotation are available and are outlined by two authors (Cooke 1991; Ries 1987) who both use orthogonal radiographs. Some groups consider rotational errors to be 'minimal' if under +/- 10° (Wright 1991).

The variation between surgeons reading the same radiographs can be quite large on it's own. Laskin conducted a study with 50 surgeons measuring the tibiofemoral angle on the same radiograph and found an interobserver standard deviation of +/- 2.1°. When asked to measure the same radiograph 2 weeks later, the intraobserver standard deviation was +/- 2.5° (Laskin 1984).

In summary, current methods of imaging the lower limb to determine frontal plane alignment using radiographs can be a major source of error for determining the correct angle for prosthesis placement. Both improvements in imaging, and adoption of standardized techniques could improve this portion of the surgical process.

1.4.3 Quantification of Implementation Error

Even if pre-planning errors on radiographs, and placement of cutting guides could be done accurately and with sufficient precision, there still remains the issue of surgical implementation. The surgeon is still responsible for performing the bone cuts, and this stage can introduce considerable error.

One paper uses Steinmann pins, which are normally used to seat the cutting guide, to determine cutting errors. When fixed by only pins (no external brace, such as with extramedullary jigs) cutting errors from 200μm to 1mm were measured (Otani 1993).

1.4.4 Rotational Alignment

Improper rotational alignment has also been identified as a factor increasing the risk of premature prosthesis failure (Rand 1991). Correct rotational alignment of knee prostheses is a complicated issue, which has not been sufficiently answered in research to date[1]. The lack of consensus, and contradictions in research findings, fuels the need for increases in accuracy, both in intraoperative procedure, and postoperative assessment. These increases in accuracy would provide research capable of more powerful conclusions.

1.4.5 Survivorship Studies

As mentioned above, pain is the most significant reason to initiate TKA. Curiously, most survivorship studies use revision as the end-point of prostheses lifespan. Pain was found to correlate well with patient satisfaction in a recent review of hip replacement (Britton 1997) and could be used as another factor in the analysis of TKA (Murray 1998).

Two articles use moderate to severe pain as the end-point for arthroplasty and report survivorships of 70% and 78% over ten years respectively (Ansari 1998; Murray 1998). The end-point is reached if pain was present anytime after the initial recovery.

Murray et al. also pointed out that falsely optimistic results are reported in many survivorship studies since the sample population often decreases to 10% of the original population. The most common reason for losing a patient is 'loss to follow-up' and death. These patients are assumed to have the same revision rate as the remaining population. The ability of the researcher to accurately measure the alignment angles is also questionable and discussed further in later sections.

1.5 Additional Problems in TKA

Intramedullary Rods

Intramedullary alignment are known to increase fat emboli during the insertion of the alignment rod (Barre 1997; Caillouette 1990; Fahmy 1990; Monto 1990; Stern 1994) ,especially in bilateral TKA (Dorr 1989; Monto 1990). Fat emboli can cause neurological damage and is the leading cause of mortality in TKA (Gleitz 1996). The

[1] Additional information has been compiled for rotational alignment of knee prostheses in TKA and can be found in Appendix A.

use of fluted rods instead of solid rods decreases the medullary pressures and the risk of fat embolisation. Venting of the medullary canal also mitigates the risk of embolisation through widening the entrance hole (Caillouette 1990). Even though progress has been made in this field, the risk of embolisation has not been eliminated (Fahmy 1990); the surgeon is still prevented from performing bilateral TKA, since the invasiveness of performing two procedures at the same time poses too high a risk.

1.6 Summary of TKA Issues

It is recognized that many factors contribute to early prosthesis failure. One is axial alignment of the lower limb. It is generally accepted that misalignment of less than 2° produces acceptable results, but surgical implementation has a standard deviation of misalignment around 2.57°. Some of the errors contributing to misalignment are radiographic technique, alignment guides, and surgical implementation. A method capable of improving frontal plane alignment would be desirable.

Rotational alignment is another factor correlated to early failure. Unfortunately, there is little consensus on the correct rotation for the components or the method of implementing it.

It is also important to note that even though alignment could be improved by removing human and mechanical error from surgical technique, surgeons provide invaluable contributions to the overall TKA procedure. In particular, dissection of the knee for bone cutting, soft tissue balancing, and general decision making around important blood vessels are all tasks which require an experienced surgeon to accomplish correctly. It is with this in mind that we consider alternatives to the current technique.

2.0 Computer Assisted Surgery

2.1 Need and Potential Benefits

Improving imaging accuracy of the lower limb, increasing frontal plane alignment accuracy, and eliminating current jigs could all improve current TKA technique by increasing overall alignment accuracy. Attempts at improving TKA in these areas using computers have been on going for the last decade and includes improved visualization of anatomical structures, increased pre-planning accuracy, and increased implementation accuracy. Robots, for example, are used to increase implementation accuracy by guiding or executing bone cutting tasks. As mentioned, aside from possible increases in prosthesis longevity, increased accuracy also allows for controlled studies into the optimal placement of the components. The elimination of intramedullary jigs can reduce the incidence of embolisation, and decrease the overall invasiveness of the procedure.

In this section, a general overview is provided of the field of computer assistance in surgery. I also review different systems developed for orthopaedic surgery and discuss the benefits, and the limitations that have prevented their commercial use in the operating room.

2.2 Classification of Computer-Assisted Surgical (CAS) Systems

Computer Assisted Systems (CAS) can be broken down into three broad categories based on the system's autonomy from the surgeon. Doing this allows us to make some generalizations regarding how appropriate they are in the operating area. The groups are: passive systems, semi-active systems and active systems (DiGioia 1998; Kienzle III 1996).

2.2.1 Passive CAS

Passive CAS is a broad definition, which includes devices that allow the surgeon to interpret anatomical geometry and relationships pre-operatively, as well as systems that allow the surgeon to passively navigate instrumentation through anatomy intraoperatively. Passive systems by definition are completely incapable of independent action and are considered surgeon-assisting devices (DiGioia 1998). In terms of the operating theatre, they are incapable of independently harming the patient or staff through physical motion, and are historically well tolerated changes to the surgical procedure.

2.2.2 Semi-Active CAS

Semi-active systems can be explained using two examples. The first is an active robot, which places non-invasive instrumentation accurately during a surgery. For instance, during TKA, an industrial robot may be used to place the cutting guides for tibial plateau resection. The second type of system uses robots that are dependent on the user for information regarding movements. These robots use powered joints to create the feeling of constraint for the user. An example would be using an industrial robot to create force feedback to a user moving the end of the manipulator. The two examples show an autonomous, but non-invasive procedure, and a system that either constrains or simulates free motion for the user using active joints. In both cases, harm should not occur to humans, but there is a reluctance to adopt robots with actively powered joints in the operating room since they posses the capability of independent motion.[2] Since the motions are controlled by software, and software is extremely difficult to guarantee reliable, there will always be questions about safety and barriers for the widespread adoption of these devices.

2.2.3 Active CAS

The last category consists solely of robots with active joints that are supposed to carry out invasive, autonomous procedures. These types of robots are considered surgeon replacing. An example of this system would be ROBODOC®, which mills the intramedullary canal of the proximal femur for total hip replacement surgery (Paul 1992). This type of system comes under intense scrutiny for safety concerns because of it's invasive and autonomous nature. Modified industrial robots in this category are the extreme case, since they are capable of producing dangerous inertia in the vicinity of the operating room staff and patient. Software reliability for motor control is, again, exceedingly difficult to prove safe.

ROBODOC has had considerable popularity in the area of hip surgery, but the hip milling is a well defined problem that can be designed to avoid endangering blood or nerve supplies. Knee replacement on the other hand has blood and nerves in the immediate proximity of the bone cuts and therefore has a greater safety requirement than with hip milling.

2.3 General Structure of CAS

2.3.1 Different Functions of CAS Systems

Traditional orthopaedic surgery can be broken down into some elementary components that allow us to examine the differences between how different CAS systems are applied. They are: planning, registration and implementation. A CAS system could be used in the planning stages to simulate surgery, while another CAS system could be used to implement the procedure.

---

[2] The theory of having a safe surgical robot, as well as some examples of safety applications in CAS are given in Appendix B.

2.3.2 Pre-planning

The planning phase usually occurs pre-operatively, involving the acquisition and processing of images (CT, MRI etc.) and their subsequent utilisation to formulate an operative plan. Some of the methods for imaging the limb are radiographs, CT scans, stereotactic fluoroscopy and MRI.[3] Computer assistance has the potential to be used as an enhanced visualization tool, and increase accuracy over conventional, unstandardized radiographic techniques.

2.3.3 Registration

Registration is the process of taking the pre-plan and relating it to the real patient. This is a crucial step, since the accuracy of pre-planning can be easily lost (Simon 1998). For example, systems employing CT pre-planning need to relate the 3D bone images to the patient lying in the operating room.

There are several techniques used to register the patient's intraoperative position to pre-surgical plans. One way is to use fiducial markers, which are anchored to bony structures. Knowing the location of the markers on the pre-planning images, as well as their physical 3D location in the operating theatre allows a mapping between the image and physical space.

2.3.4 Implementation

In CAS, implementation is the actual action of the surgery. For example, the implementation stage for the ROBODOC® system is the femur milling.

2.4 CAS Research in Surgery

Computer assisted surgical systems are used in a wide range of orthopaedic surgeries such as spinal pedicle screw insertion, total hip and knee arthroplasty, distal locking of intramedullary nails, acetabular fractures and femoral fracture fixation (Simon 1998). I outline a few of the systems relevant to TKA.

2.4.1 Davies et al., ACROBOT

Davies et al. (Imperial College, England) describe a robot that allows the surgeon to perform bone cuts by moving a force controlled handle attached to the bone saw. While making the bone cuts, the surgeon backdrives motors. Free motion of the bone saw is allowed by the motors until the system senses that the user is moving into a restricted area (a 'zone of exclusion'). These restricted areas are based on pre-planning using a CT scanner. The system then provides force feedback appropriate to the direction of the cut and proximity to soft tissue structures. Since the robot enforces programmable constraints using *active* motors, it is known as an "Active Constraint Robot" (ACROBOT). The system is still in the design and testing stages (Davies 1997).

The benefit of this system is that it couples the accuracy of computer assistance with the tactile sense and expertise of the human operator. In terms of classification, ACROBOT is considered semi-active CAS, since it uses active motors to enforce constraints. The use of active motors introduces safety concerns, which may make it harder to introduce the system.

2.4.2 Fadda et al., Italy

Researchers in Italy modified an industrial robot to perform bone cuts autonomously. The system uses three implanted landmarks for registration to the pre-operative CT Scan (Wang 1994). The markers in the OR are recognised by guiding the robot arm to the general area and having the robot search for the local markers. Thus far, their work has focused on validating the cutting force model so the system can detect the end of a bone cut.

This system is considered active CAS, and once again raises serious questions regarding safety.

---

[3] For more information regarding imaging techniques, see Appendix C.

2.4.3 Leitner, Cinquin et al., France

Leitner et al. recognised problems of using a CT-scan for planning, such as cost and radiation exposure, and designed a less costly alternative (Leitner 1997). Their system uses a 3D localizer called Optotrak, which spatially locates infra-red diodes. Many systems locate anatomical features through tracking invasive pins mounted rigidly on bony structures. Leitner proposes using a traumatic approach by determining all of the landmarks of the lower limb through a "range of motion" technique. The bone cuts are implemented using a modified cutting guide, which is anchored to the bone and adjusted for the correct tilt and height based on computer feedback.

This method is completely intraoperative and produced initial results in cadaver studies of 2° maximum errors. From a safety perspective, this passive CAS could be easily adopted as a surgical technique. A potential limitation is that Optotrak requires an unimpeded view of the markers, which is not always convenient in a busy operating room. Although this system does ensure more accurate placement of the cutting guide, implementation errors by the surgeon, such as skewing of the saw blade, are not eliminated.

2.4.4 Troccaz et al., France

PADyC is a passive system that uses clutches to control the direction taken by the end effector of a serial linkage (Troccaz 1996). Two clutches are used for each direction of motion at a joint. When engaged, they prevent rotational movement in one direction for a joint. By engaging both clutches, no motion occurs at the joint. The PADyC robot uses high speed switching of the clutches to achieve the desired direction of motion.

This system uses passive guidance and could be easily used in an operating theatre. As with ACROBOT, PADyC is best suited to enforcing zones of exclusion. This system has been implemented in a serial 2 DOF device.

2.4.5 Book et al., P-TER

Another type of passive device is called a Passive Trajectory Enhancing Robot, or P-TER (Book 1996; Gomes 1997). This manipulator uses clutches and brakes to guide the user's motions along a path. The potential application would be guidance of surgical equipment in the OR to increase precision and accuracy. Like ACROBOT, and PADyC, the system is best suited to enforcing zones of exclusion. It also represents an excellent opportunity to couple computers and humans.

Although inherently passive, the clutches and brakes create a jerky constraint, which requires high switching rates to achieve adequate control. Thus far, P-TER has only been implemented in a 2 DOF device.

2.4.6 Peshkin et al., Cobots

Researchers at Northwestern University in Chicago invented a new breed of collaborative robots, or cobots (Peshkin 1996). They are capable of enforcing smooth, programmable, virtual constraints on motion using frictional transmission elements. To date, a 2D unicycle, a 3D tricycle, and a 2 DOF parallelogram cobot exist (Gillespie 1999; Wannasuphoprasit 1997).

They are passive and could be used as 6 DOF guidance devices, but the current research has not produced a manipulator in more than 3 dimensions systems. They are light, because they require no heavy motors for actuation, and from a safety perspective, they avoid many of the safety issues that prevent other systems from succeeding.

2.5 Summary of CAS Issues

In the context of TKA, using CAS to increase accuracy represents a great opportunity. In particular, using guidance systems for the implementation of more accurate bone cuts is especially promising. Many devices are active, and fall short because of safety concerns. Although some passive systems, such as PADyC and P-TER

could be applied to TKA, they are better suited to implementing zones of exclusion, instead of enforcing smooth constraints, as would be needed for cutting planes in TKA.

Cobots provide an ideal way of coupling the accuracy of computer assistance with the experience of a surgeon. They can provide stiff, smooth, and arbitrary virtual constraints. Current designs are limited because they are not minimally constrained and require force sensing to selectively align the programmable constraints. Although the possibility exists for 6 DOF design, one has not been constructed yet, and no transmission device has been constructed to support a parallel architecture, which offer superior stiffness and accuracy in a surgical setting.

3.0 Layout of Thesis

Our ultimate goal is to build a cobot for improving bone cutting accuracy. To achieve this goal, a method of accurately defining the mechanical axis of the lower limb must be established. Secondly, since cobots possess the necessary characteristics for passively guiding bone cuts, a cobot must be built. The beginning of this thesis presents some early work on accurately defining the lower limb mechanical axis. The major contributions of the thesis are in the remainder of the thesis, which concentrates on creating the framework for developing a cobot well suited to assisting bone cuts. Final construction or evaluation of the accuracy of the cobot is necessary, but beyond the scope of this thesis.

The second chapter presents the work on an improved probe that could be used to robustly locate rounded anatomical landmarks, such as the condyles of the knee. This paper was a joint effort between Kevin Inkpen, Dr. Antony Hodgson and myself, and is published in the conference proceedings for MICCAI '98 (Inkpen K.B. 1998). This work tries to address the need for an accurate method of defining the mechanical axis of the lower limb. Work by Kevin Inkpen further addresses reducing errors introduced by inaccurate mechanical axis determination (Inkpen, 1999).

Subsequent research was focused on the development of a cobot for guiding bone cuts. This work aims to reduce implementation errors, which are not addressed by the mechanical axis definition work. The main contributions of this thesis are in the development of a key element for a parallel cobot; the novel concept of minimally constrained cobots; and a control strategy for controlling these minimally constrained cobots. By performing this research, the foundation is laid for the creation of a cobot capable of assisting bone cutting in knee surgery.

Chapter 3 contains the development of the prototype transmission for a parallel cobot. In this chapter I discuss the prototype in terms of its capabilities, limitations, and areas of future work.

In chapter 4, I propose a strategy for controlling minimally constrained cobots. In particular, the control theory is developed and applied in a few basic examples. Practical simulations are also presented to show the controller working under 3 dimensional conditions.

Chapter 4 was submitted in February 2000, to the ASME Haptics Symposium while Chapter 3 is written as an unpublished journal paper. In both cases, the papers are collaborations between Dr. Antony Hodgson and myself, where I am the primary author.

References

Ansari, S, Ackroyd, CE, and Newman, JH: Kinematic posterior cruciate ligament-retaining total knee replacements. A 10-year survivorship study of 445 arthroplasties. Am.J.Knee.Surg. 11:9, 1998.

Bargren, JH, Blaha, JD, and Freeman, MA: Alignment in total knee arthroplasty. Correlated biomechanical and clinical observations. Clin.Orthop. 178, 1983.

Barre, J, Lepouse, C, and Segal, P: Embolism and Intramedullary Femoral Surgery. Rev.Chir.Orthop.Reparatrice.Appar.Mot. 83:9, 1997.

Book, W, Charles, R, Davis, H, and Gomes, M. Concept and implementation of a passive trajectory enhancing robot. Proceedings of the ASME Dynamic Systems and Control Division American Society of Mechanical Engineers, Dynamic Systems and Control Division 58, 633-638. 1996. Atlanta, GA. Proceedings of the 1996 ASME International Mechanical Engineering Congress and Exposition. Conference Proceeding

Britton, AR, Murray, DW, Bulstrode, CJ, McPherson, K, and Denham, RA: Pain levels after total hip replacement: their use as endpoints for survival analysis. J.Bone Joint Surg.Br. 79:93, 1997.

Caillouette, JT and Anzel, SH: Fat embolism syndrome following the intramedullary alignment guide in total knee arthroplasty. Clin.Orthop. 198, 1990.

Cates, HE, Ritter, MA, Keating, EM, and Faris, PM: Intramedullary versus extramedullary femoral alignment systems in total knee replacement. Clin.Orthop. 32, 1993.

Chao, EY, Neluheni, EV, Hsu, RW, and Paley, D: Biomechanics of malalignment. Orthop.Clin.North Am. 25:379, 1994.

Chao, EY and Sim, FH: Computer-aided preoperative planning in knee osteotomy. Iowa.Orthop.J. 15:4-18:4, 1995.

Cooke, TD, Scudamore, RA, Bryant, JT, Sorbie, C, Siu, D, and Fisher, B: A quantitative approach to radiography of the lower limb. Principles and applications. J.Bone Joint Surg.[Br.] 73:715, 1991.

Cooke, TD, Siu, D, and Fisher, B: Use of standardized radiographs to identify the deformities associated with osteoarthritis. In AnonymousRecent Developments in Orthopaedic Surgery. Manchester, Manchester University Press, 1987, p. 264.

Davies, BL, Harris, SJ, Lin, WJ, Hibberd, RD, Middleton, R, and Cobb, JC: Active compliance in robotic surgery--the use of force control as a dynamic constraint. Proceedings of the Institution of Mechanical Engineers, Part H 211:285, 1997.

Dennis, DA, Channer, M, Susman, MH, and Stringer, EA: Intramedullary versus extramedullary tibial alignment systems in total knee arthroplasty. J.Arthroplasty 8:43, 1993.

DiGioia, AM, Jaramaz, B, and Colgan, BD: Computer assisted orthopaedic surgery. Image guided and robotic assistive technologies. Clin.Orthop. 8, 1998.

Dorr, LD, Merkel, C, Mellman, MF, and Klein, I: Fat emboli in bilateral total knee arthroplasty. Predictive factors for neurologic manifestations. Clin.Orthop. 112, 1989.

Evans, PD, Marshall, PD, McDonnell, B, Richards, J, and Evans, EJ: Radiologic study of the accuracy of a tibial intramedullary cutting guide for knee arthroplasty. J.Arthroplasty 10:43, 1995.

Fahmy, NR, Chandler, HP, Danylchuk, K, Matta, EB, Sunder, N, and Siliski, JM: Blood-gas and circulatory changes during total knee replacement. Role of the intramedullary alignment rod. J.Bone Joint Surg.[Am.] 72:19, 1990.

Figgie, HE, Goldberg, VM, Figgie, MP, Inglis, AE, Kelly, M, and Sobel, M: The effect of alignment of the implant on fractures of the patella after condylar total knee arthroplasty. J.Bone Joint Surg.[Am.] 71:1031, 1989.

Gillespie, RB, Colgate, JE, and Peshkin, M: General framework for cobot control. Proceedings IEEE International Conference on Robotics and Automation 3:1824, 1999.

Gleitz, M, Hopf, T, and Hess, T: Experimental studies on the role of intramedullary alignment rods in the etiology of fat embolisms in knee endoprostheses. Z.Orthop.Ihre.Grenzgeb. 134:254, 1996.

Gomes, MW and Book, WJ. Control approaches for a dissipative passive trajectory enhancing robot. IEEE ASME International Conference on Advanced Intelligent Mechatronics , 92. 1997. IEEE ASME International Conference on Advanced Intelligent MechatronicsBı. Conference Proceeding

Green, SA and Green, HD: The influence of radiographic projection on the appearance of deformities. Orthop.Clin.North Am. 25:467, 1994.

Inkpen K.B. Precision and Accuracy in Computer Assisted Total Knee Replacement. 12-1999. University of British Columbia. Thesis/Dissertation

Inkpen K.B., Emrich RJ, and Hodgson A.J. Probe Design to Robustly Locate Anatomical Features. Lecture Notes in Computer Science 1496, 335-342. 1998. New York, Springer-Verlag. Medical Image Computing and Computer Assisted Intervention, MICCAI'98. Conference Proceeding

Ishii, Y, Ohmori, G, Bechtold, JE, and Gustilo, RB: Extramedullary versus intramedullary alignment guides in total knee arthroplasty. Clin.Orthop. 167, 1995.

Jeffery, RS, Morris, RW, and Denham, RA: Coronal alignment after total knee replacement. J.Bone Joint Surg.[Br.] 73:709, 1991.

Jessup, DE, Worland, RL, Clelland, C, and Arredondo, J: Restoration of limb alignment in total knee arthroplasty: evaluation and methods. J.South.Orthop.Assoc. 6:37, 1997.

Jiang, CC and Insall, JN: Effect of rotation on the axial alignment of the femur. Pitfalls in the use of femoral intramedullary guides in total knee arthroplasty. Clin.Orthop. 50, 1989.

Kienzle III, TC, Stulberg, SD, Peshkin, MA, Quaid, A, Lea, JT, Goswami, A, and Wu, C: A Computer-Assisted Total Knee Replacement Surgical System Using a Calibrated Robot. In Taylor, R., Lavallee, S., Burdea, G.C., and Mosges, R., (eds.): Computer Integrated Surgery. Cambridge, MA, USA, MIT Press, 1996, p. 409.

Kim, W, Rand, JA, and Chao, EY: Biomechanics of the KNee. In Rand, J.A., (ed.): Total Knee Arthroplasty. New York, USA, Raven Press, 1993, p. 9.

Krackow, KA: The Technique of Total Knee Arthroplasty. St.Louis, USA, The C.V. Mosby Company, 1990,

Laskin, RS: Alignment of Total Knee Components. Orthopedics. 7:62, 1984.

Leitner, F, Picard, F, Minfelde, R, Schulz, H-J, Cinquin, P, and Saragaglia, D. Computer Assisted Knee Surgical Total Replacement. Troccaz, J, Grimson, E, and Mosges, R. 629-638. 1997. Grenoble, France, Springer - Verlag. CVRMed - MRCAS Proceedings '97. Conference Proceeding

Lennox, DW, Cohn, BT, and Eschenroeder, HCJ: The effects of inaccurate bone cuts on femoral component position in total knee arthroplasty. Orthopedics. 11:257, 1988.

Monto, RR, Garcia, J, and Callaghan, JJ: Fatal fat embolism following total condylar knee arthroplasty. J.Arthroplasty 5:291, 1990.

Moreland, JR: Mechanisms of failure in total knee arthroplasty. Clin.Orthop. 49, 1988.

Moreland, JR: Intramedullary Versus Extramedullary Total Knee Instrumentation. In Goldberg, V.M., (ed.): Controversies of Total Knee Arthroplasty. New York, Raven Press, 1991, p. 185.

Murray, DW and Frost, SJ: Pain in the assessment of total knee replacement. J.Bone Joint Surg.Br. 80:426, 1998.

Otani, T, Whiteside, LA, and White, SE: Cutting errors in preparation of femoral components in total knee arthroplasty. J.Arthroplasty 8:503, 1993.

Paul, HA, Mittlestadt, B, Bargar, WL, Musits, B, Taylor, RH, Kazanzides, P, Zuhars, J, Williamson, B, and Hanson, W. A surgical robot for total hip replacement surgery. Proceedings IEEE International Conference on Robotics and Automation 1., 606-611. 1992. New York, IEEE. Proceedings IEEE International Conference on Robotics and Automation. Conference Proceeding

Pereira, DS, Jaffe, FF, and Ortiguera, C: Posterior cruciate ligament-sparing versus posterior cruciate ligament-sacrificing arthroplasty. Functional results using the same prosthesis. J.Arthroplasty 13:138, 1998.

Peshkin, M, Colgate, JE, and Moore, C: Passive robots and haptic displays based on nonholonomic elements. Proceedings IEEE International Conference on Robotics and Automation 1:551, 1996.

Petersen, TL and Engh, GA: Radiographic assessment of knee alignment after total knee arthroplasty. J.Arthroplasty 3:67, 1988.

Rand, JA and Ilstrup, DM: Survivorship analysis of total knee arthroplasty. Cumulative rates of survival of 9200 total knee arthroplasties. J.Bone Joint Surg.[Am.] 73:397, 1991.

Rathjen, KW: Surgical treatment. Total knee arthroplasty. Am.J.Knee.Surg. 11:58, 1998.

Reed, SC and Gollish, J: The accuracy of femoral intramedullary guides in total knee arthroplasty. J.Arthroplasty 12:677, 1997.

Ries, M and O'Neill, D: A method to determine the true angulation of long bone deformity. Clin.Orthop. 191, 1987.

Simmons, EDJ, Sullivan, JA, Rackemann, S, and Scott, RD: The accuracy of tibial intramedullary alignment devices in total knee arthroplasty. J.Arthroplasty 6:45, 1991.

Simon, DA and Lavallee, S: Medical imaging and registration in computer assisted surgery. Clin.Orthop. 17, 1998.

Stern, SH, Sharrock, N, Kahn, R, and Insall, JN: Hematologic and circulatory changes associated with total knee arthroplasty surgical instrumentation. Clin.Orthop. 179, 1994.

Teter, KE, Bregman, D, and Colwell, CWJ: Accuracy of intramedullary versus extramedullary tibial alignment cutting systems in total knee arthroplasty. Clin.Orthop. 106, 1995a.

Teter, KE, Bregman, D, and Colwell, CWJ: The efficacy of intramedullary femoral alignment in total knee replacement. Clin.Orthop. 117, 1995b.

Troccaz, J and Delnondedieu, Y: Semi-active guiding systems in surgery. A two-DOF prototype of the passive arm with dynamic constraints (PADyC). Mechatronics 6:399, 1996.

Wang, T, Fadda, M, Marcacci, M, Martelli, S, Dario, P, and Visani, A: Robotized surgeon assistant. Proceedings of the IEEE/RSJ/GI International Conference on Intelligent Robots and Systems 2:862, 1994.

Wannasuphoprasit, W, Gillespie, RB, Colgate, JE, and Peshkin, MA. Cobot control. Proceedings IEEE International Conference on Robotics and Automation 4, 3571-3576. 1997. New York, IEEE. Proceedings of the 1997 IEEE International Conference on Robotics and Automation, ICRA. Conference Proceeding

Wright, JG, Treble, N, and Feinstein, AR: Measurement of lower limb alignment using long radiographs. J.Bone Joint Surg.[Br.] 73:721, 1991.

Chapter 2 - Probe Design to Robustly Locate Anatomical Features

Abstract. Computer-assisted surgical techniques which seek to avoid relying on CT or MRI scans often require intraoperative location of anatomical features. The conventional optoelectronic probe measures a cloud of points on the feature surface, but the resulting location estimate is subject to bias and variation due both to local deformations in the surface and to measurement noise. We compare three probe designs – the conventional point probe, a flat probe and a V-probe – and show that all exhibit strong directional variability when estimating the centre of a quarter arc. We also show that the V-probe design is superior in tests on a 2D image, reducing the variability in localizing a femoral condyle by 50%.

1.0 Introduction

We are currently developing a technique for computer-assisted total knee replacement (TKR) surgery which does not require preoperative CT scans (similar to Leitner, 1997). Certain variations of our approach require approximating centres of the posterior portions of the femoral condyles, which have been shown to closely fit spherical surfaces (Kurosawa, 1985). We propose to pass an optoelectronic digitizing probe over the condylar surfaces and fit a sphere to them, taking the centre of the fitted sphere as the condylar centre. This paper concentrates on the reliability of this latter process. In particular, we wish to characterize the repeatability with which we can define these centres.

Commercially available probes usually have a point or small (about 2 mm diameter) spherical end that touches the subject (see Figure 6). Such probes are versatile in that they can be used define points on surfaces with detailed concave and convex features. In our application, however, the subject surface is generally convex with local flaws that do not represent the ideal sliding surface that we are trying to locate. We suggest alternative probe designs that may be less sensitive to local deformations in the articular surface and may lead to more reliable estimates of the condylar centres. For general registration applications as discussed in (Simon, 1994), the effect of probe design should be considered when the goal is to quickly gather data that accurately constrain a convex feature.

In this paper we investigate using a probe with a flat contact surface to provide data as a series of tangent lines (rather than points) as the probe is swept along a surface. We also investigate the use of a V shaped probe that returns a series of local curvature bisector lines from a similar scan. A best fit 'centre' point of the contour can be found by minimizing an appropriate cost function. At this stage, we are interested in the repeatability of an estimated centre point location found from a single scan of a surface.

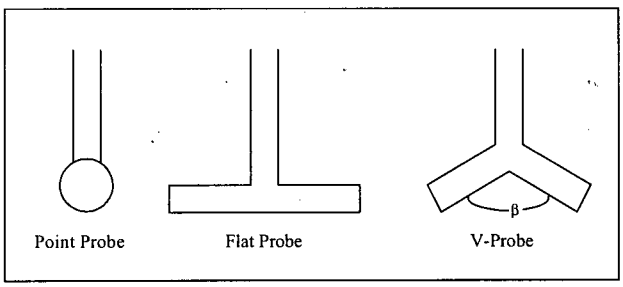

Figure 6. Different Probe Designs

We simulate 1000 scans each over two different 2D test curves using each probe design and compare the standard deviations from the mean of the resulting estimated centres. We show that the V-probe exhibits significantly less standard deviation, thus better repeatability, than the other two designs.

2.0 Methodology

We simulated tests of a point probe, a flat probe, and V-probes with a variety of β angles (10° increments from 120° to 170°) on two reference curves:

I. The circumference of a true quarter arc with a 13 mm radius.

II. The posterior-distal quadrant of a 2D contour of the lateral condyle of a human femur (~13 mm radius) obtained from a sagittal MRI of a 31 year old female with no significant knee pathology.

For both curves, we simulated sweeping the probes across a 90° range, added measurement noise, and found the best-fit centre point by minimizing an appropriate cost function (see Sections 2.1 - 2.3) using MATLAB's Nelder-Mead simplex method.

For each probe type and each reference curve, we ran 1000 simulated scans which resulted in 1000 estimated centres. We then computed the standard deviation of centre point location as a measure of the repeatability of the probe type.

We simulated the intraoperative process of acquiring points along the curve as a rotation of the probe about the origin (roughly the centre of the curve) with the radius being determined by the requirement that the probe maintain contact with the curve. In practice the surgeon would tend to start with the probe at one end of the curve with zero velocity, sweep through approximately 90°, and come to rest at the end of the curve. We therefore calculated the sampling position vector θ as:

$$\theta = \theta_s + (\theta_f - \theta_s)(1 + \sin(\pi((t / t_s) - 0.5))) / 2 \qquad (1)$$

where t is a vector of time steps from t = 0 to total scanning time (t_s) with a step size of (sampling frequency)$^{-1}$. θ_s and θ_f are the start and finish angles of the scanned range. In this study t_s = 1 s, sampling freq. = 60 Hz, θ_s = 90°, and θ_f = 180° for all simulations and all angles are measured positively CCW from the x axis. For the V-probes, the range of θ was reduced to $[\theta_f - (\pi - \beta)/2] - [\theta_s + (\pi - \beta)/2]$ to ensure that there was no contact outside of the sampled range used for the other probes.

During each simulation, we added white noise with $\sigma = 0.02$ radians to each sampling position θ to ensure that we were not always sampling at the same points. We also added white noise with $\sigma = 0.2$ mm to all (x,y) coordinate data to simulate the measurement errors of a typical optoelectronic localizer. Assuming a distance of 120 mm from the probe surface to the probe markers, a corresponding white noise with $\sigma = 0.20/120 = 0.0017$ radians was added to all angular data.

2.1 Point Probe

To estimate the centre of the best-fit circle, we computed the contact point of the probe to the surface at each sampling position θ and added noise as described above, producing a set of noisy data points (x_p, y_p). With candidate circles defined by their centre coordinates and radius (x_c, y_c, r_c), the point probe cost function 'PPCF' is the sum of squared normal distances from the points to the candidate circle:

$$PPCF = \Sigma\,(r_c - ((x_p - x_c)^2 + (y_p - y_c)^2)^{1/2})^2 \qquad (2)$$

2.2 Flat Probe

For the flat probe, we calculated the contact point between the probe and the surface contour, (x_f, y_f), and the angle of the probe face, (α), at each sampling position θ and added noise. The flat probe cost function 'FPCF' is the sum of squared distances along the lines coperpendicular to both the candidate circle and the flat probe:

$$FPCF = \Sigma\,((x_f - x_t)\sin\alpha + (y_f - y_t)\cos\alpha)^2 \qquad (3)$$

where (x_t, y_t) are the co-ordinates of the point on the candidate circle whose tangent is parallel to the probe face.

2.3 V-Probe

At each sampling position θ, the V-shaped probe contacts the surface contour in two places and the centre of any 'local' best-fit circle at this sampling position must lie somewhere along the bisector of the V. As the probe is swept along the surface contour over the scanned range, these bisectors form a set of lines intersecting near the centre of an overall best-fit circle. The angle of each bisector, γ, and a point on the bisector at the apex of the V, (x_v, y_v), form the data set and have noise applied. The cost function 'VPCF' expresses the sum of the squared normal distances between the candidate centre point, (x_c, y_c), and the bisectors:

$$VPCF = \Sigma \left((x_v - x_c) \sin \gamma - (y_v - y_c) \cos \gamma \right)^2 \qquad (4)$$

Note that in this case, we cannot explicitly estimate the radius of the arc.

3.0 Results

3.1 True Arc

Figures 7 and 8 show the 1000 estimated arc centres for the point probe and 140° V-probes respectively. The results for the flat probe are comparable to the point probe and so are not shown here. Note the extended distribution of these estimates along the axis of symmetry of the arc.

To evaluate the repeatability of each probe design, standard deviations in centre point location were found for two different measures: 'Sym. Axis' is the standard deviation measured parallel to the bisector of the scanned range. 'Perp. Axis' is the standard deviation measured perpendicular to the bisector of the range.

Table 1. Standard deviations of centre point location from true arc

	Sym. Axis (mm)	Perp. Axis (mm)
Point	0.134	0.043
Flat	0.116	0.041
V120	0.137	0.025
V130	0.112	0.027
V140	0.080	0.027
V150	0.070	0.028
V160	0.062	0.030
V170	0.056	0.028

3.2 Posterior-Distal Condyle Image

As in the first test, 1000 scans were simulated with each probe design on the same set of points representing the contour of a sagittal section through the distal femur. All three probe designs proposed a different mean centre point location (See Fig. 9).

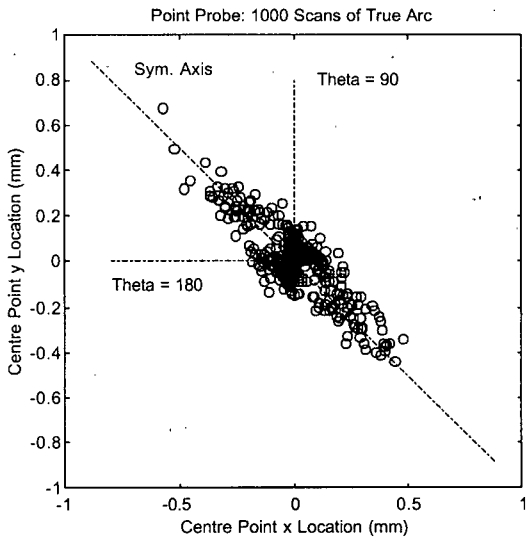

Figure 7. Point probe: Estimated centre point locations for true arc.

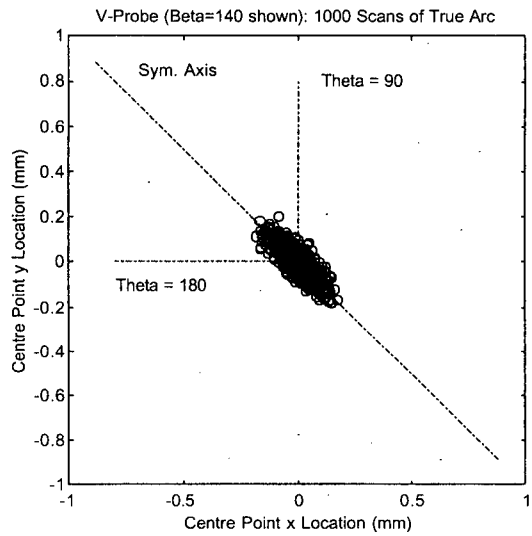

Figure 8. V140 Probe ($\beta = 140°$): Estimated centre point locations for true arc.

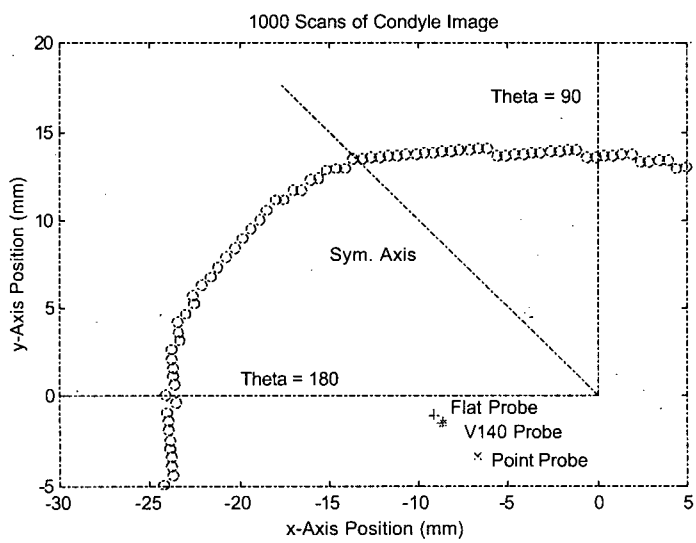

Figure 9. Average centre point estimation for each probe design on condyle image.

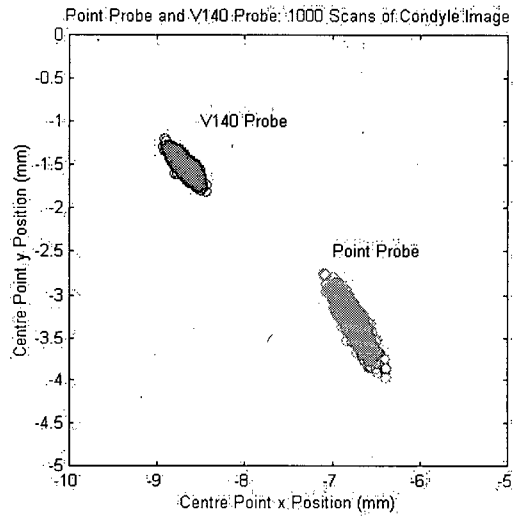

Figure 10. Distribution of centre point estimates for point and V140 probes on condyle image.

Repeatability of each probe design was calculated again and is shown in Fig. 11.

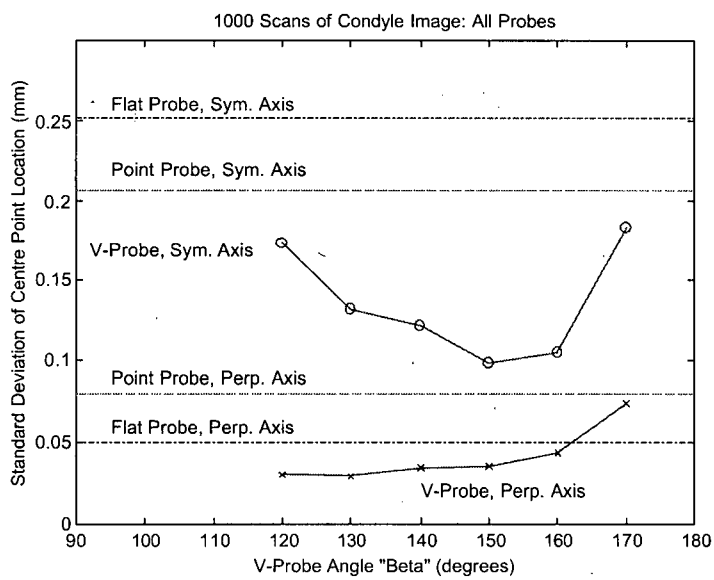

Figure 11. Standard deviation of centre point location on condyle image, all probe designs.

4.0 Discussion

The extent of the cloud of centre point estimates derived from the true arc indicates sensitivity to measurement noise. All three probes exhibited 2-5X more deviation along the arc's axis of symmetry than perpendicular to it. This can be explained by looking at the cost functions: For the point and flat probes, the circle descriptors involve three parameters (x, y, and r), where negative displacements of (x,y) along the arc's axis of symmetry coupled with increases in radius (r) will cause the least change in cost. For the V-probe, (x,y) are found to minimize the summed distances to the radial data lines (set of bisectors), so displacements in the direction 'most parallel' to the

average data line (ie. along the arc's axis of symmetry) will cause the least change in cost. The SD of the flat probe's centre estimate distribution is ~15% lower than that of the point probe, but the V-probe's distributions showed further reductions of 35-50% in SD, showing that it is markedly less sensitive to measurement noise. Increased V-probe angles (β) produced significantly lower standard deviations of the point location along the axis of symmetry but had no significant effect perpendicular to the axis of symmetry.

On the condyle image, all three probes again showed maximum SD along the axis of symmetry of the best fit arc. There is a small difference in SD between the point and flat probes, although this time the point probe has the smallest value. As on the true arc, the V-probes with β in the range of 130° to 160° showed SD's up to 50% lower than the point and flat probes along both axes and showed less pronounced variation along the axis of symmetry, creating a more circular cloud of points.

The mean centre point estimated by the point probe was located about 3 mm from those estimated by the flat and V-probes (Figs. 9 & 10). It appears that this difference is caused by the near flat region over the first half of the scanned range in this particular contour. The point probe will record many points on this flat region, forcing the best fit circle downwards and to a greater radius. In contrast, contact points for the flat and V-probes will move counterclockwise onto the downward slope of the contour earlier in the scanned range (assuming the probe surfaces are large enough), reducing the influence of the flat region.

5.0 Conclusions

The V-shaped probe design enables us to locate a characteristic feature of condylar geometry (i.e., the centre of a best fit arc) with up to half the variability of a flat probe or conventional point probe. The variability of this localization is greatest along the arc's axis of symmetry. We are planning to extend this study to three dimensions, where the V-probe will be replaced by a three-faced pyramidal probe. Such a probe is also likely to have benefits in other registration applications.

Acknowledgements

We thank Dr. Boris Flak of the UBC Department of Radiology for help in obtaining the MRI scan of the knee, Roger Tam of the UBC MAGIC Lab for assistance in converting the image for use in this project, and Robert W. McGraw of the UBC Department of Orthopaedics for discussions on TKR procedure.

References

Leitner, F., Picard.F., Minfelde, R., Schulz, H-J., Cinquin P., Saragaglia D.: Computer Assisted Knee Replacement Surgical Total Replacement. In: Troccaz, J., Grimson, E., Mosges, R. (eds): CVRMed-MRCAS '97. Lecture Notes in Computer Science, Vol. 1205. Springer-Verlag, Berlin Heidelberg New York (1997) 627-638.

Kurosawa, H., Walker, PS.,Abe, S.,Garg, A., Hunter, T. : Geometry and Motion of the Knee for Implant and Orthotic Design. Journal of Biomechanics (1985); 18 (7): 487 - 499.

Simon, D.A., Hebert, M.., Kanade T.: Techniques for Fast and Accurate Intra-Surgical Registration. In: DiGioia, A.M., Kanade, T.,Taylor, R. (eds.): MRCAS '94, Vol. 1. Pittsburgh, Pennsylvania. (1994) 90-97.

Chapter 3 - A CVT Element for Parallel Cobots

Abstract. Cobots are inherently passive devices which constrain the motions of an end-effector powered by external means (often a human user). Previous cobot designs have relied either on a wheel or a rotational continuously variable transmission (CVT) to couple joint velocities; these elements are best suited to planar or serial manipulator designs. In this paper, we describe the design of a new CVT mechanism which is well suited for parallel manipulators and outline a potential application in computer-assisted surgery.

1.0 Introduction

Cobots, or **CO**llaborative ro**BOT**s, are a comparatively recent innovation in robot design which use orientable constraints to guide the motion of the end-effector. Since the motors that orient these constraints do not supply any power to the cobot's links, a cobot is intrinsically passive and relies on an external source for motive power. This innate passivity greatly enhances safety in applications where one wishes to blend the intelligence of a human operator with the precision and strength of a robot by having the two cooperate on a manipulation task. Indeed, in its initial applications (e.g., in guiding auto parts such as doors to the correct place during assembly), the motive power comes from a human operator.(Wannasuphoprasit 1998) There is also an important cost advantage in using a cobot in place of a robot in a standalone application: Moore *et al* have suggested that a single power-supplying motor can be integrated into a cobotic design to eliminate most of the high-power actuators that would otherwise be required in a conventional robotic design with a similar architecture.(Moore 1999)

Cobots implement their constraints using friction drive elements with continuously-variable drive ratios which are altered under computer control to allow the end-effector to track the desired path. We can think of a trike under computer control. The computer can control the steering wheel of the trike, however no amount of turning the wheel can cause motion to occur. Instead, the control is left up to the operator who can then pedal when, and at what speed, they desire.

To date, cobots have been designed using one of two major continuously variable transmission (CVT) designs: a wheel and a rotational drive. The wheel has been used in carts which travel on a planar surface: Colgate (1996) *et al* have designed perhaps the simplest possible cobot – a two-dimensional unicycle which controls the planar position of a handle without regard to orientation – while Wannsuphoprasit (1997) *et al* have designed a three-dimensional cart called 'Scooter', which can control its angular orientation in addition to its planar position.(Colgate 1996; Wannasuphoprasit 1997) In contrast to the wheel, the rotational drive relates rotational velocities of two nearby shafts and has been used to build a 3D cobotic arm with a substantially serial architecture; in this design, all drives are located in the cobot's base and passive drivetrains link them to the distal joints whose motions they control.(Moore 1999)

Parallel robots represent an important third robotic architecture distinct from planar carts and serial arms, but neither CVT design described above is particularly appropriate for this class of robots. These parallel architectures move by changing the length of a series of legs, all attached between the base and the end effector of the manipulator. As wheel CVTs relate linear velocities, a parallel CVT would require a device to relate the velocities of each of the legs of a parallel manipulator. We propose a new kind of CVT that is well-suited for parallel cobots. Our own interest in parallel cobots stems from an ongoing project in computer-assisted knee surgery; in surgical applications, parallel designs have advantages over serial designs because of their limited workspace, higher accuracy and greater stiffness.(Brandt 1996; Arai 1990) In addition, parallel designs can typically carry greater end-effector loads and can be easily designed with all the motors in the base, which simplifies the sterilization procedure for robots used in the operating room. The most common form of parallel

architecture is known as the Stewart Platform, shown in Figure 12 (Fichter 1996). To convert such a design to a cobot, we must have a CVT which can constrain the relative lengthening or shortening velocities of (typically adjacent) leg pairs.

As with all CVT designs, a CVT for a parallel platform should have the following characteristics:

1. A means to vary the transmission ratio without causing motion of the end-effector
2. A range of motion consistent with the desired workspace of the end-effector
3. A continuously variable transmission ratio which smoothly passes through zero
4. The ability to change the preloads on the friction drive elements to enable the design to handle different end-effector loads

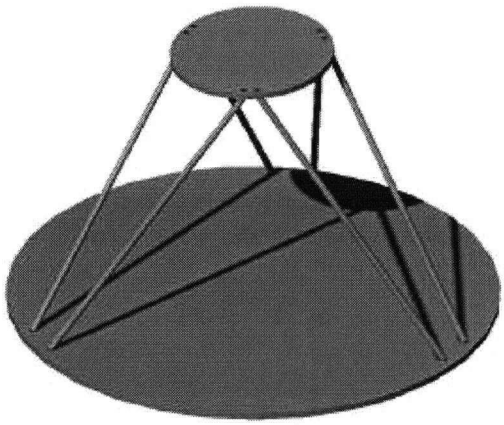

Figure 12. Schematic of Stewart platform showing layout of base, end-effector and linear actuators.

2.0 CVT Concept

2.1 Physical Components: Description & Purpose

Criterion #1 above implies that there is no feedthrough of motive power from the steering motors to the end-effector. Our proposed CVT element (see Figure 13) is based on a cylindrical leg link which is attached to the end-effector through a spherical bearing (not shown) and so is free to spin about its axis without transmitting any significant torque to the end-effector. At the base, the leg is also pressed against a spherical surface attached to a shaft constrained to rotate about a fixed axis. The leg is driven axially when the contact point between the sphere and leg (assuming a no-slip condition) has a velocity component along the leg.

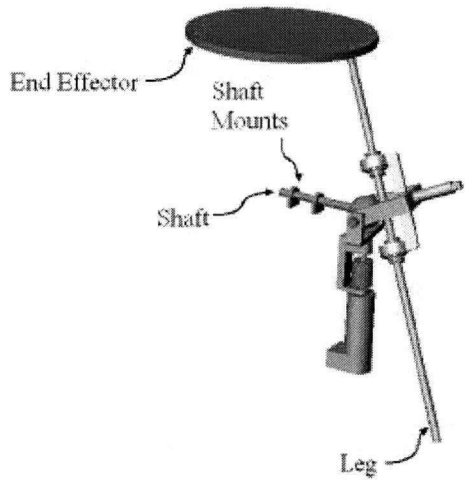

Figure 13. Overview of proposed CVT design for parallel cobots (note: shaft diameter is smaller than will actually be used).

The leg is also free to roll on the surface of the sphere without exerting a force on the end-effector; in this way, the steering action can be decoupled from the driving forces. The steering, which sets the relationship between the shaft velocity and leg velocity, is guided by a yoke mechanism whose axis passes through the centre of the sphere and which requires negligibly small actuating torques from the steering motor to turn. By using this yoke to change the contact point between the leg and the sphere, we can change the ratio between the axial displacement of the leg and the rotational displacement of the shaft.

Finally, in a complete cobot, the shaft rotations of multiple CVT elements could be coupled to one another through some common drive element such as a bevel gear or the flat wheel drive proposed by Moore.(Moore 1999)

2.2 CVT Operation

To understand how this CVT functions, consider the situation in which the fixed shaft is spinning at a constant angular velocity, ω_0 (see Figure 14) and the steering yoke is holding the leg against the sphere with the contact point somewhere on the vertical plane which contains the shaft axis. If the leg is also vertical, the contact point will be at the distal tip of the sphere and its velocity will be zero, so the leg will neither extend nor spin on its own axis. If the end-effector moves so that the leg remains in the vertical plane but the contact point shifts away from the horizontal plane, the contact point's velocity will become non-zero because its velocity is given by $\omega_0 R_b$, where R_b is the perpendicular distance of the leg link from the axis of the rotating ball. Despite this non-zero contact point velocity, the leg will simply spin around its axis without lengthening or shortening because the velocity of the contact point is perpendicular to the leg's axis.

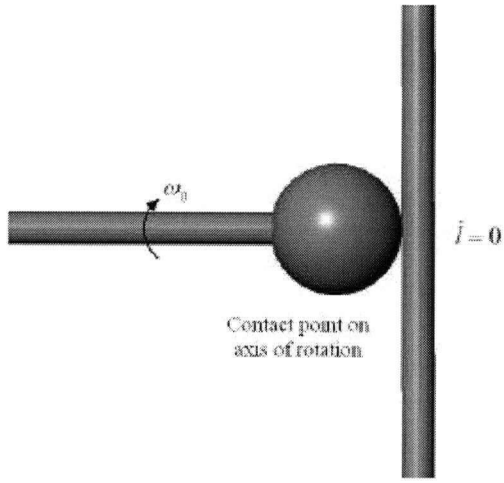

Figure 14. Leg position which results in zero axial velocity (note: many structural details omitted for clarity).

However, if we turn the yoke in one direction or another so that the contact point shifts away from the vertical plane through the shaft axis (see Figure 15), then the projection of the contact point's velocity on the leg's axis is no longer zero and the leg will either lengthen or shorten while simultaneously spinning about its axis. Note that in Figure 15 we have decomposed the contact point velocity into components parallel to the leg's axis and perpendicular to it. The perpendicular velocity divided by the radius of the leg represents the leg's angular velocity, while the projection along the leg axis represents the lengthening or shortening velocity. Lengthening or shortening can also occur if the contact point is in the vertical plane, but off the horizontal plane, *and* if the pivot point connecting the leg to the end-effector moves out of the vertical plane, since this will make the contact point's velocity no longer perpendicular to the leg axis.

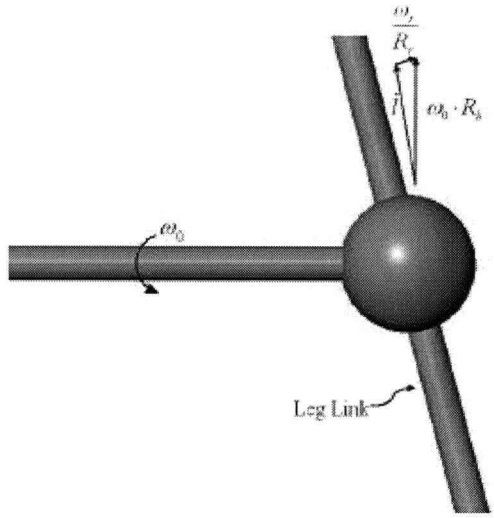

Figure 15. Leg position which results in significant axial velocity.

If the contact point shifts to 90° around the ball (roughly the position shown in Figure 15) and if the leg moves into a plane perpendicular to the shaft axis, then it will lengthen at its maximum rate and will cease spinning about its axis. If the yoke were turned in the opposite direction, the leg's translation would reverse direction, so the ratio of leg speed to shaft speed can smoothly pass through zero.

2.3 Range of Motion

The parallel cobot described here has some range of motion limitations not shared by conventional parallel manipulators. In particular, the parallel cobot does not have telescoping legs, in contrast to the typical Stewart platform design which uses hydraulic cylinders or other linear actuators. As seen in Figure 13, when the parallel cobot's legs shorten, they must extend past the CVT. Since the space into which they intrude must be kept clear of obstacles and since we require space below the CVTs in which to mount the steering motors, it is reasonable to restrict the cobot's legs to point inwards above the base, which implies that the workspace limits occur whenever one or more legs reach the vertical. This also implies that the cobot's end-effector must be smaller than its base in order to allow any movement in the horizontal plane. Also, when the end-effector moves downward, the leg extensions below the cobot's base may come into contact with one another; this implies both that the base points must be spaced a reasonable distance apart from one another and that the vertical workspace of a parallel cobot will likely be modest.

3.0 Calculating The Jacobian

3.1 Conventional Parallel Manipulators

In order to formulate control laws for a parallel cobot, we must establish the relationship between the leg and end-effector velocities (i.e., the jacobian of the manipulator) for a given end-effector position. In particular, if l is the length of a given leg, x is a 6-vector describing the end-effector position (e.g., the Cartesian position of the centre of the end-effector and three Euler angles describing its current rotation), and $J(x)$ is the 1x6 jacobian for the given leg, then the leg velocity is given in terms of the end-effector velocities by

$$\dot{l} = J(x)\dot{x} \tag{5}$$

In a conventional parallel manipulator, the jacobian computation is straightforward since the legs are attached to both the base and the end-effector using spherical bearings or ball joints and the distances between the centres of these pivot points are easily computed given the position of the end-effector. For example, given the centres of the pivot points on the base and the end-effector (P_b and P_e), we can compute the jacobian as follows:

First, define a vector from the base pivot to the end-effector pivot:

$$L = P_e - P_b \tag{6}$$

We normalize L to create a unit vector z pointing to the end-effector pivot.

$$z = \frac{L}{\|L\|} \tag{7}$$

The influence of end-effector rotations on L is computed by the cross product of the vector from the centre of the end-effector (P_c) to the pivot point and z:

$$s = P_e - P_c \tag{8}$$

$$J = \begin{bmatrix} z^T & (s \times z)^T \end{bmatrix}$$

3.2 Parallel Cobots

In contrast to conventional parallel manipulators, the leg length (defined for a parallel cobot as the distance between the pivot at the end-effector and the centre of the corresponding drive sphere at the base) can change not only because the contact point velocity has an axial component along the leg (analogous to shortening in a conventional parallel robot), but also because of rotation of the leg about the sphere. This effect is illustrated in Figure 16 for a planar device – the end-effector displacement δx can be decomposed into components both axially along the leg (δx_a) and perpendicular to the line connecting the contact point to the pivot on the end-effector (δx_r); note that these velocity components are not quite perpendicular to one another because of the finite diameter of the leg. Note also that because the rotational component increases the distance between sphere and pivot centres, the axial displacement in this case slightly overestimates the actual change in L computed using the jacobian defined in Equation 8.

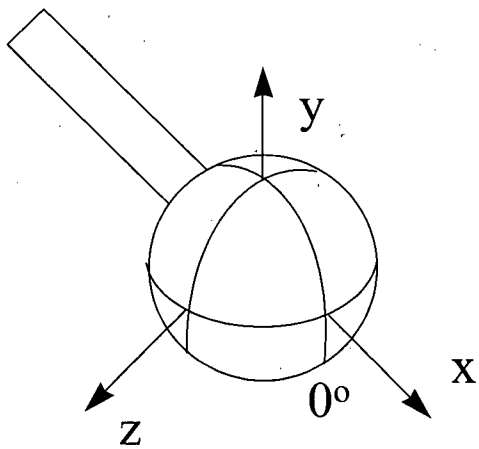

Figure 16. Coordinate frames used to compute position of contact point.

In order then to calculate the differential driveshaft rotation corresponding to a given differential end-effector displacement, we must take account both of the effect described above and of the relationship between the axial leg displacement and shaft rotation at the current steering angle. In contrast to Moore's rotational CVT design in which the transmission ratio depends only on the steering angle (because the driveshaft and the output shaft maintain a fixed spatial relationship to one another), in our design the drive ratio depends on the end-effector position.

3.2.1 Finding Contact Point

The first step in computing the drive ratio is to determine the current contact point between the sphere and the leg. To do this, we set up a Cartesian coordinate system with its origin at the centre of the sphere and simultaneously define a latitude/longitude system on the surface of the sphere (see Figure 17). We take the polar line to lie along the y axis (north pole in the $+y$ direction) and define 0° longitude at the point where the x axis pierces the sphere.

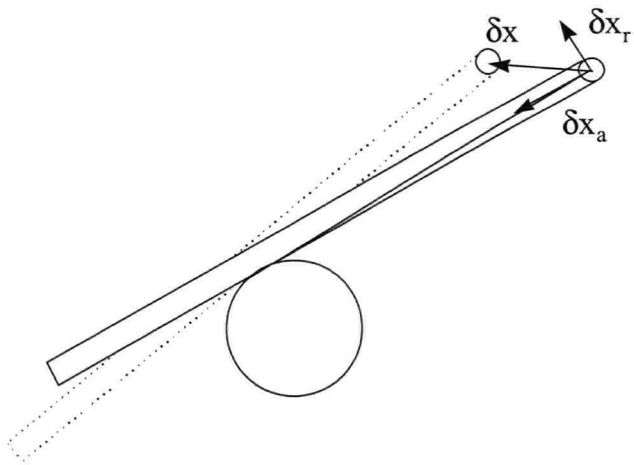

Figure 17. Decomposition of end-effector movement into components due to axial translation and rotation about the contact point. Note that these components are not perpendicular to one another.

Given these coordinate systems and referring to Figure 18, we see that the contact point lies directly in line with the secondary yoke at a longitudinal position 90° away from the cross-axis of the primary yoke. The steering angle of the primary yoke therefore directly determines the longitude, α, of the contact point.

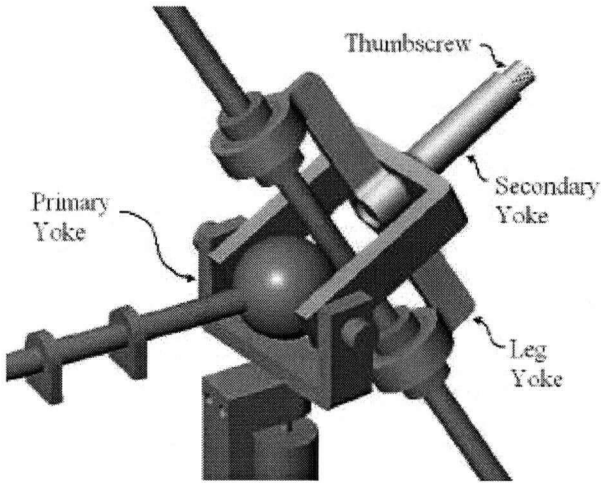

Figure 18. Detail of yoke mechanisms which support the leg and determine the point of contact between the leg and sphere.

The latitude of the contact point is determined by the projection of two lines into the plane P defined by the great circle of constant longitude which passes through the contact point (see Figure 19). The first line is L, as defined earlier: the line which connects the end-effector pivot to the sphere centre. The second line is L', which runs from the end-effector pivot along the axis of the leg. Consider a third line, L'', which is perpendicular to L' and passes through the sphere's centre. We define β as the angle between L'' and the projection of L into P and solve for β as $\arccos((R+r)/\|L_P\|)$, where R is the radius of the sphere, r is the radius of the leg, and L_P is the projection of L into P (see Figure 20). The latitude of the contact point is $180°-\gamma-\beta$, where γ is the angle between L_P and the horizontal (easily computed knowing L_P). Given the latitude and longitude of the contact point, it is straightforward to calculate its cartesian coordinates, $\underline{R}$.

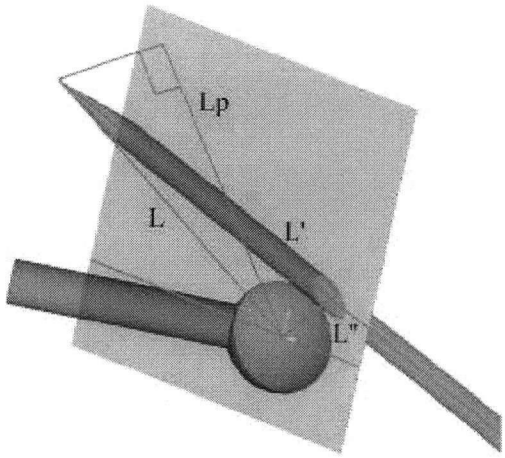

Figure 19. Geometry used to determine contact point coordinates. The plane, *P*, which passes through both poles and the contact point between the leg and drive sphere is shown in grey.

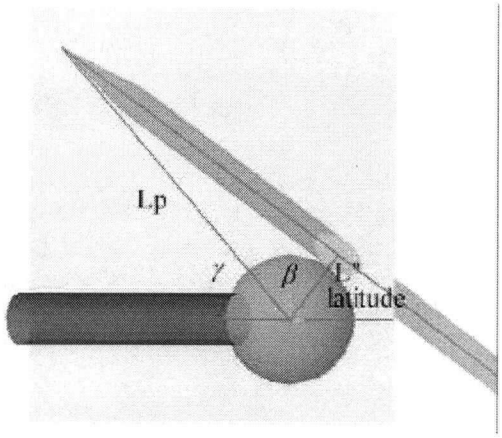

Figure 20. Front view of plane *P* described in Figure 8 showing the definitions of the angles used to compute the latitude of the contact point.

3.2.2 Computing Drive Ratio

To determine the relationship between the leg's axial velocity and the shaft rotation speed, we note that the velocity of the contact point is given by $\omega_0 \times \underline{R}$, where ω_0 is the angular velocity of the fixed shaft (see Figure 15). We define a second plane P_t which is tangent to the sphere at the contact point (not shown in Figure 19 for clarity in the previous section). Looking normal to this plane, we see that P projects as a line in P_t. We define the pivot angle ϕ as the angle in P_t between the projections of P and the leg axis. The axial velocity of the leg is the dot product of this velocity and a unit vector along the leg axis and has a magnitude equal to $\|\omega_0 \times \underline{R}\| \cos \phi$.

To summarize, given the current end-effector position and a specified end-effector displacement, we compute the location of the contact point between the leg and the sphere. We then decompose the the differential end-effector displacement into components due to rotation and pivoting about the contact point and translation along the leg axis in order to find the differential axial displacement of the leg. Knowing the direction of the velocity of

the contact point, we can compute the differential rotation of the shaft needed to accommodate the specified end-effector displacement.

4.0 Design Details

Successful implementation of the concept described above requires careful attention to a number of construction details. In particular, there is a fundamental contradiction inherent in the design: the leg must have a high friction connection with the driving sphere, but must move freely (i.e., without apparent friction) with respect to the seating mechanism which supports and guides the leg. Simultaneously satisfying these two goals is the greatest mechanical challenge in the design. To maximize the useful workspace of the cobot and the range of drive ratios which can be achieved, it is also important to pay attention to the yoke details. Finally, we consider the selection of the motor and electronic interface components.

4.1 Seating Mechanism

The purpose of the seating mechanism is threefold: (1) to constrain the contact point between the leg and the sphere to a desired longitude and (2) to apply sufficient pressure across the interface to allow frictional forces to support the required end loads while (3) allowing the leg to self-align with the end-effector regardless of the current location of the contact point.

Considering the self-alignment issue first, we observe that if the steering motor is fixed and the end-effector moves, the seating mechanism must allow the leg to accommodate the end-effector motion such that the leg remains axially loaded, rather than being placed into bending. To do this, we provide the leg yoke (see Figure 18) to allow the leg to pivot about its contact point and the secondary yoke to allow the leg to rotate about the sphere. The axis of the leg yoke remains pointing at the same longitude on the sphere under both of these self-alignment motions. When the secondary yoke rotates, the leg moves axially relative to the leg yoke; linear bearings are provided to allow for this translation.

The primary yoke is driven by the steering motor and shifts the contact point to a new longitude. To enable the leg to move to this new position without sliding on the surface, we must provide some support to allow the leg to roll; needle bearings in the leg yoke acting in concert with a spherical bearing at the end-effector connection allow for this rolling action.

Finally, the leg yoke itself can translate along the secondary yoke's barrel and is spring-loaded against the drive sphere by a compression spring mounted inside the barrel; the force in the spring can be adjusted by the thumbscrew shown.[4]

4.2 Material Selection

Because the CVT is a friction drive mechanism, we would like the interface between the sphere and the leg to have a high coefficient of friction, yet allow for comparatively free rolling of the leg across the sphere's surface. A high coefficient of friction also simplifies the design of the seating mechanism described above because it reduces the seating force required to sustain a given end-effector load.

Our current design uses stainless steel tube for the leg and a rubber coated sphere. We selected steel for the tube because the leg also has to be supported by linear bearings and they run best on a steel shaft. The alternative, a steel sphere and a rubber-coated leg, would require major changes to the design of the leg yoke's linear bearings.

---

[4] Detailed shop drawings for each part of the CVT are included in Appendix F.

The requirement for a high coefficient of sliding friction along with a low coefficient of rolling friction is difficult to satisfy. One technique for achieving the latter is to have two stiff elements to minimize contact deformations, with one coated with a high friction material to enhance sliding friction. It is somewhat difficult to obtain an inexpensive, easily applied and durable friction coating, but we found that a reasonable compromise could be reached by using mouse balls, which are constructed using a comparatively thin rubber coating applied over a stainless steel core. We have found that the coefficient of friction of such an interface to be on the order of 0.3-0.4.

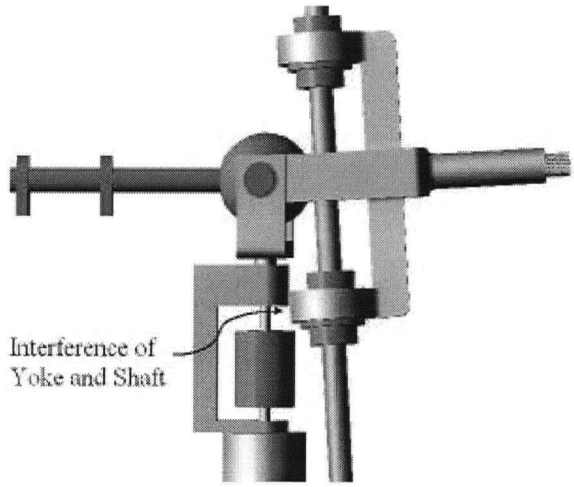

Figure 21. Leg yoke impinging on motor support.

4.3 Yoke Details

There is one place in the primary yoke and two in the leg yoke where structural elements limit the operating range of the CVT.

The primary yoke controls the longitude of the contact point; ideally, the contact point should be adjustable throughout a range of ±90° from neutral. In practice, since the primary yoke has bearings at ±90° from the contact point, the range is more limited. The degree of limitation depends on the relative sizes of the sphere, the yoke bearings and the shaft. Figure 21 shows how the yoke can impinge on the shaft at one extreme. We can achieve maximum range of motion by minimizing the sizes of the shaft and the yoke bearings and housings relative to the sphere.

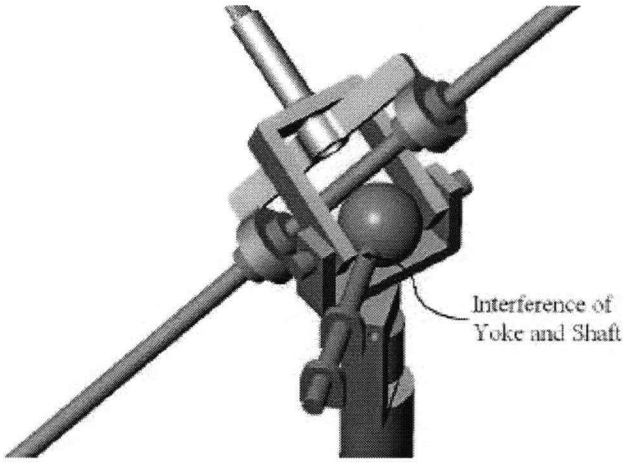

Figure 22. Primary yoke at extreme of motion where it impinges on the driving shaft.

The leg yoke, as mentioned earlier, accommodates shifts in the end-effector position by pivoting about the contact point. The current design allows for roughly ±30° of pivoting, which is probably sufficient for our application; greater rotations are prevented by the leg yoke impinging on the secondary yoke.

The final place where impingement occurs is between the leg yoke and the motor supports when the leg reaches its most vertical position (see Figure 22).

4.4 Motor and Electronic Interface Selection

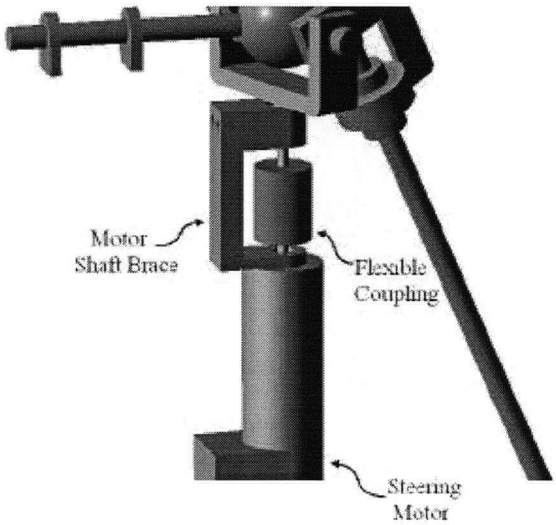

Figure 23. Flexible coupling to isolate motor from seating forces.

By choosing a material for the sphere with a low coefficient of rolling friction against a steel tube, we were able to minimize the size of the motor, since it only has to overcome the small amount of friction required to roll the leg around the sphere. We chose a small Maxon A-max 3.5 W motor, which has a maximum continuous torque of 0.3 Nm. Because the seating mechanism can apply comparatively high forces to the yoke, we explicitly designed

the yoke bearings to take these loads and isolated the motor from them using a flexible coupling which has high torsional stiffness (see Figure 23).

To control the motor, we selected a Maxon linear servo controller and a Humusoft MF604 DIO card with four channels each of encoder input and D/A output. The motors are equipped with optical encoders (100 counts per revolution) and a 19:1 planetary gearhead, so the effective resolution of the encoders is 1900 counts per revolution. The low-level motor controller is based on a simple PD controller implemented using MATLAB's Realtime Workshop; we also intend to use this environment to implement the complete controller for the full cobot[5].

5.0 Potential Application

We have designed this prototype with surgical applications in mind. In particular, we are developing a computer-assisted technique for total knee arthroplasty aimed at decreasing or eliminating the incidence of early failure of the prostheses due to inaccuracies in implant placement.(Inkpen K.B. 1999) Some of our recent results (manuscript in preparation) have indicated that the greatest contribution to variability in our computer-guided technique is the accuracy with which the surgeon can implement the bone cuts indicated by the system. We therefore anticipate that it will be necessary to supplement our current system with some means of guiding the surgeon's bone-cutting tools more precisely. Active robots have been suggested for this task, but have not yet been widely accepted, in part because of their costs, but also in large measure because of safety concerns.(Cain 1993; Ellenby 1994; Taylor 1991; Bainville 1996; Taylor 1991; Bainville 1996) One way to alleviate these concerns is to develop a mechanism that passively constrains a surgeon's motions while relying on the surgeon for all motive power, hence the appeal of the cobotic approach, particularly if it can be coupled with a parallel architecture.

Aside from cobots, two other devices have been proposed which provide passive virtual programmable constraints on user motion. The first is a passive trajectory enhancing robot (P-TER), which uses a combination of clutches and brakes to regulate the coupling between the two joints.(Book 1996; Gomes 1997) The other is the Passive Arm with Dynamic Constraints (PADyC), which uses clutches and free wheels to constrain each joint to the intended path.(Troccaz 1993b) Both systems have only been prototyped in two degrees of freedom (DOF) and neither have been applied to a parallel architecture. The PADyC, in particular, is best suited for preventing entry into regions of the workspace rather than closely constraining motion to a trajectory or plane, a task for which cobots are well suited.

6.0 Conclusions

The completion of this cobot will represent both the first parallel cobot and the first one to operate in 6-space. We intend to refine our design to optimize the size of the cobot's workspace and to develop a reusable and sterilizable end-effector suitable for use in surgery. The proposed CVT is readily integrated into a parallel design in which the CVTs are arranged symmetrically at the base and driven by a common drive plate, as described in Moore (1999), which opens the way for a powered parallel cobot with a single primary drive motor.(Peshkin 1996)

---

[5] For more information regarding the control hardware for the cobot, see Appendix D.

References

Arai, T, Cleary, K, Nakamura, T, Adachi, H, and Homma, K. Design Analysis and Construction of a Prototype Parallel Link Manipulator. IEEE International Workshop on Intelligent Robots and Systems , 205-212. 1990. New York, IEEE. IEEE International Workshop on Intelligent Robots and Systems. Conference Proceeding

Bainville, E and Cinquin Ph. Method and system for determining the fixation point on the femur of a crossed ligament of the knee. 166,032(5,564,437), 1-6. 10-15-1996. Germany. Patent

Book, W, Charles, R, Davis, H, and Gomes, M. Concept and implementation of a passive trajectory enhancing robot. Proceedings of the ASME Dynamic Systems and Control Division American Society of Mechanical Engineers, Dynamic Systems and Control Division 58, 633-638. 1996. Atlanta, GA. Proceedings of the 1996 ASME International Mechanical Engineering Congress and Exposition. Conference Proceeding

Brandt, G, Rau, G, Radermacher, K, Lavallee, S, Erbse, S, and Staudte, HW. Development of a robot with optimized kinematics for the treatment of bone structures. Annual International Conference of the IEEE Engineering in Medicine and Biology Proceedings (1), 236-237. 1996. IEEE. Annual International Conference of the IEEE Engineering in Medicine and Biology Proceedings. Conference Proceeding

Cain, P, Kazanzides, P, Zuhars, J, Mittelstadt, B, and Paul, H: Safety considerations in a surgical robot. Biomedical Sciences Instrumentation 29:291, 1993.

Colgate, JE, Wannasuphoprasit, W, and Peshkin, MA. Cobots: robots for collaboration with human operators. Proceedings of the 1996 ASME International Mechanical Engineering Congress and Exposition 58, 433-439. 1996. Atlanta, GA. Proceedings of the International Mechanical Engineering Congress and Exhibition. Conference Proceeding

Ellenby, SB: Safety issues concerning medical robotics. Computing and Control Division Colloquium on Safety and Reliability of Complex Robotic Systems 1, 1994.

Fichter, EF: A Stewart Platform-Based Manipulator: General Theory and Practical Construction. The International Journal of Robotics Research 5:157, 1996.

Gomes, MW and Book, WJ. Control approaches for a dissipative passive trajectory enhancing robot. IEEE ASME International Conference on Advanced Intelligent Mechatronics , 92. 1997. IEEE ASME International Conference on Advanced Intelligent MechatronicsBı. Conference Proceeding

Inkpen K.B. and Hodgson A.J. Accuracy and Repeatability of Joint Centre Location in Computer-Assisted Knee Surgery. Image Computing and Computer Assisted Intervention (MICCAI '99) , 1072-1079. 2-1999. New York, Springer-Verlag. Medical Image Computing and Computer Assisted Intervention (MICCAI '99). Conference Proceeding

Moore, CA, Peshkin, MA, and Colgate, JE. Design of a 3R cobot using continuously variable transmissions. Proceedings IEEE International Conference on Robotics and Automation 4, 3249-3254. 1999. New York, IEEE. Proceedings of the 1999 IEEE International Conference on Robotics and Automation, ICRA99. Conference Proceeding

Peshkin, M, Colgate, JE, and Moore, C: Passive robots and haptic displays based on nonholonomic elements. Proceedings IEEE International Conference on Robotics and Automation 1:551, 1996.

Taylor, RH, Paul, H, Kazanzides, P, Mittelstadt, B, Hanson, W, Zuhars, J, Williamson, B, Musits, B, Glassman, E, and Bargar, WL. Taming the Bull: Safety in a Precise Surgical Robot. Proceedings IEEE International Conference on Robotics and Automation 1, 865-870. 1991. New York, IEEE. Proceedings IEEE International Conference on Robotics and Automation. Conference Proceeding

Troccaz, J and Lavallee, S. Alternative to actuated robots sand passive arms in medical robotics. Proceedings of the Annual Conference on Engineering in Medicine and Biology 15, 934-935. 1993. New York, IEEE. Proceedings of the 15th Annual International Conference of the IEEE Engineering in Medicine and Biology Society. Conference Proceeding

Troccaz, J, Lavallee, S, and Hellion, E. Passive arm with dynamic constraints: A solution to safety problems in medical robotics? Proceedings of the IEEE International Conference on Systems, Man and Cybernetics 3, 166-171. 1993. New York, IEEE. Proceedings of the IEEE International Conference on Systems, Man and Cybernetics. Conference Proceeding

Wannasuphoprasit, W, Akella, P, Peshkin, M, and Colgate, JE. Cobots: a novel material handling technology. Proceedings of the 1998 ASME International Mechanical Engineering Congress and Exposition , 1-7. 1998. Fairfield, NJ., ASME. Proceedings of the 1998 ASME International Mechanical Engineering Congress and Exposition. Conference Proceeding

Wannasuphoprasit, W, Gillespie, RB, Colgate, JE, and Peshkin, MA. Cobot control. Proceedings IEEE International Conference on Robotics and Automation 4, 3571-3576. 1997. New York, IEEE. Proceedings of the 1997 IEEE International Conference on Robotics and Automation, ICRA. Conference Proceeding

Chapter 4 - Controlling Minimally-Constrained Parallel Cobots

Abstract. Cobots are a new class of manipulators that derive motive power from a human operator while constraining the direction of end-effector motion by orienting passive constraints under computer control. They allow the operator to control execution speed and environmental interactions during an interactive task, while adding the positioning precision associated with traditional active robots. This synergetic union of human and computer control strengths is desired in fields such as surgical robotics (our application area of interest) where the surgeon would prefer not to hand over control of a procedure to an autonomous robot. Previous cobot designs intrinsically allow only zero or one degree of freedom of motion, but there are some surgical tasks (such as using a bone saw to cut a plane in knee replacement surgery) where allowing two or three degrees of freedom is desireable. While it is possible to add degrees of freedom to a fully-constrained robot, this results in a system with more actuators than are necessary. We introduce here the concept of minimally-constrained cobots for multiple degree of freedom tasks such as planar cutting and outline a general framework for controlling such devices. In particular, we illustrate our control algorithms using a planar cart example and discuss how they might be applied to potential designs for three-dimensional parallel cobots intended for surgical applications.

1.0 Introduction

Conventional robots are powered, autonomous devices that have been successfully used in a wide variety of industrial applications to increase the efficiency of repetitive, well structured tasks. In less structured settings (such as surgery), the complexity, variability, or safety requirements of the task may make it impossible to replace a human operator with an autonomous device. Nonetheless, it would often be desirable to marry the precision of a robot with the decision making skills of a human operator. For example, we are working to improve the accuracy of bone cuts in knee replacement surgery. It is clear that the positioning accuracy of the artificial implants significantly affects its lifespan (Figgie 1989; Jeffery 1991; Rand 1991; Moreland 1988). The variability associated with the existing jig-based procedures is large enough that a significant fraction of ostensibly correctly implanted prostheses are in fact malaligned (Inkpen K.B. 1999). Computer-assisted techniques have been proposed to more accurately identify the correct cutting planes in an assortment of orthopaedic procedures (Leitner 1997; Moody JE 1998; Tonetti 1998), but the variability of the surgeon's subsequent bone cut is still unacceptably large for TKA (Inkpen K.B. 1999). A robot would be able to make these cuts accurately enough, but because of the complexity of the soft tissue structures and the proximity of the blood vessels and nerves supplying the lower limb, no surgeon would be willing to allow a robot to make the bone cuts autonomously. What is needed is a system that passively constrains the bone saw to the desired cutting plane while leaving the surgeon to control motion and cutting forces in that plane.

At least three kinds of devices have been proposed to meet this need. PADyC uses high speed switching of clutches to enforce programmable constraints (Troccaz 1996). PADyC has been implemented in a 2 DOF serial manipulator. P-TER is similar, using high speed switching of clutches and brakes to achieve constraint on user motion (Book 1996; Gomes 1997). This system has also been implemented on a 2 DOF manipulator. ACROBOT relies on force feedback to keep the user constrained to predetermined planes (Davies 1997). Past efforts in creating motion constraints involved force sensing of the user's input and responding with an appropriate reaction forces created by active robot joints. This gives the user the feeling of constraint, but involves actively powered joints capable of developing dangerous inertia. It is also very hard to prove that controlling software will be completely reliable. Of these two, only PADyC is truly passive, but both it and ACROBOT are best suited to implementing zones of exclusion and are less appropriate for constraining an end-effector to a line or plane.

More recently, a third class of guiding robot has been developed which is capable of constraining motion to a desired line or plane while ensuring that all motive power comes from a human operator (Colgate 1996). These collaborative robots, or *cobots*, were originally designed to address occupational injuries and hazards on auto assembly lines, but a much wider variety of applications have been envisioned, including applications in surgery (Wannasuphoprasit 1998). In contrast to ACROBOT, cobots are intrinsically passive. They are unable to move independently under any circumstances because the computer-controlled actuators simply orient frictional constraints; they cannot supply any energy in the directions of allowed motion. Because of this feature, the users'

actions can be guided by the cobot without a concern that the robot can "go wild". Cobots therefore offer great potential for a synergistic blending of human expertise and robotic precision.

Perhaps the easiest way to envision how a cobot operates is to consider a computer-steered tricycle. The user could pedal the trike at whatever speed they wish, but the computer would be responsible for monitoring the progress of the trike and steering according to a predefined plan. Since the steering of the device is the only input under computer control, and since no amount of steering action can cause the trike to move if the user is not pedaling, the device is inherently passive.

All cobots rely on a friction mechanism to enforce non-holonomic constraints between two components of velocity. In the case of the tricycle, a steering wheel determines the direction in which the contact point between the wheel and the ground moves. Two other continuously variable transmission (CVT) designs currently exist.(Moore 1999; Wannasuphoprasit 1997) Researchers at Northwestern University have designed a CVT which relates the speeds of two fixed shafts and have applied it to a 3DOF serial cobotic device, and we have recently designed one suitable for linking the extension or retraction speeds of legs in a parallel mechanism which we envision as being suitable for surgical applications (Emrich 2000).

To date, cobots have been implemented as zero or one degree of freedom (DOF) devices (Wannasuphoprasit 1997). They can move in at most one direction at a given instant, that direction being determined by the configuration of the CVTs. As the CVTs are reconfigured, the direction of allowed motion also changes. A path following algorithm has been developed for constraining the guided object to a one dimensional line in the taskspace (Gillespie 1999).

However, we have already pointed out that some tasks require higher degrees of freedom. In addition to the bone-cutting example discussed above in which planar motion is desired, NWU researchers have discussed a parts handling application in which there is a region within which the user can freely maneuver the part, but as the part approaches another part to which it is to be connected, the desired path becomes one-dimensional (Wannasuphoprasit 1998). If the cobot is to constrain the part to a one-dimensional final path in a planar manipulation task, then it must be capable of applying two constraints on the motion. If this is the case, however, then the cobot is instantaneously capable of motion only in a single direction. If the user applies forces perpendicular to this direction, the cobot must be able to sense this and realign the constraints to allow motion in the indicated direction. If the cobot actually has three independent constraints (e.g., three wheels on a planar cart), then it intrinsically has zero degrees of freedom; to get the cobot to move at all, the constraints must be properly aligned with one another.

The NWU researchers have taken this approach to emulating multiple degrees of freedom in a cobot. While there is considerable flexibility in this approach to change the apparent degrees of freedom of the device and to implement regions within which the user can maneuver, there are some disadvantages as well. First, it requires the use of a force sensor, which increases the expense of the cobot. Second, force data is often noisy and must be filtered before being used to alter a constraint; this introduces a time lag into the system's response which interferes with the perception of free motion in higher dimensions. Finally, some tasks, such as our knee surgery task, do not require that we switch back and forth between lower and higher dimensional motion regions; in such cases, the increased number of actuators is redundant and adds to the expense and complexity of the cobot. We therefore propose an approach to designing cobots with a minimal number of constraints (and hence actuators) for tasks with an intrinsic dimension greater than one. In particular, we outline a framework for controlling such minimally-constrained cobots, provide examples of applying the control algorithms to planar carts of various configurations used in various tasks, and discuss how we might extend the control algorithms to a parallel cobot we have proposed for knee surgery.

2.0 Implementation of Minimally-Constrained Cobots

2.1 Example System: A Planar Cart

The simplest possible minimally-constrained cobot would move in a three-dimensional taskspace and be subject to a single non-holonomic motion constraint. The wheel is our CVT and would provide a way of setting the relationship between x and y velocities. Because the wheel is non-holonomic, it does not explicitly constrain the configuration of the cart (ie. Position and orientation). For example, the wheels on a car prevent it from moving sideways, but do not prevent the car from driving in a circle and coming to rest beside the original position.

Throughout this paper, we will be using a planar cart to illustrate the various elements of the controller. This cart is shown in Figure 24. We will define its position using a 3-vector consisting of the coordinates of the control point {x,y} and the cart's orientation {θ}. There is a steering wheel positioned a distance Lx along the x axis of a frame attached to the cart (note: we can assume without loss of generality that the frame's x axis points from the control point to the centre of the steering wheel, which we will also refer to as the wheel point). We define the steering angle, α, as the angle that the steering wheel makes with the local x axis (X_c). In addition to the steering wheel, we imagine that their are two casters on the cart which support it on the planar surface but which do not impose constraints parallel to the plane. The cart therefore has two instantaneous degrees of freedom: it can pivot about the wheel's contact point with the ground, or it can move such that the motion of the wheel point is in the direction which the wheel is pointing. Because the constraints are non-holonomic, however, we must express the cart's position using three coordinates.

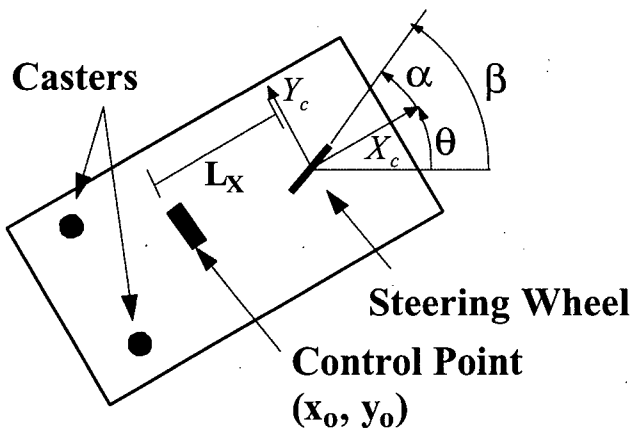

Figure 24. Diagram of Planar Minimally Constrained Cart

2.2 Controller Overview

To design our cobot controller, we borrow from the framework for a one-dimensional path-following cobot laid out by Gillespie et al.(Gillespie 1999) We define our control goal in taskspace and develop transformations from taskspace to configuration space (if applicable) and from there into the coupling spaces where the steering elements can affect the motion. We then design control laws to alter the steering angles for the continuously variable transmissions used in cobots to orient the frictional constraints.

Figure 25 illustrates the relationships between the various spaces used to design the controller for the planar cart. It is important to note that the steering angle, α, influences the differential motions in the coupling space. Devices with more CVT's will have one coupling space for each additional CVT; for each coupling space, there will be a corresponding steering angle which will control differential motion in that coupling space.

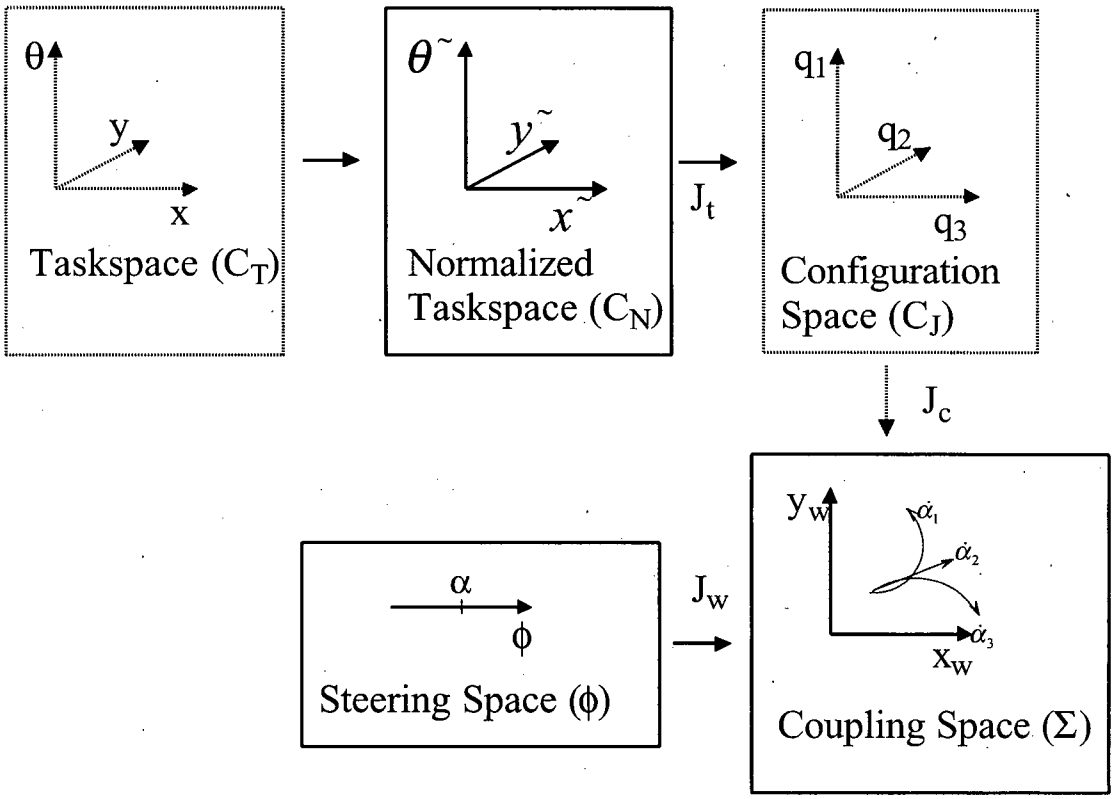

Figure 25. Relationships (including jacobians) between the various spaces used to control a planar cart.

2.3 Target Manifold

To design a controller for the cart (or any minimally-constrained cobot), we must first describe the subspace to which we wish to confine its motion. The taskspace (C_T) is an n-dimensional space containing all possible configurations of the end-effector. In the case of the planar cart, our taskspace has 3 dimensions, representing one rotational and two translational coordinates. We define the target manifold (TM) to be an m-dimensional subspace of C_T (where $1<m<n$) to which we wish to constrain motions of the end-effector. This manifold can in general be either planar or a more complex surface and can also evolve with time.

In our planar cart example, the target manifold could be the plane shown in Figure 26, which represents a simple static 2D target manifold in a 3D taskspace. This particular target manifold specifies that we would like our guided object to travel along the line x = y with arbitrary orientation.

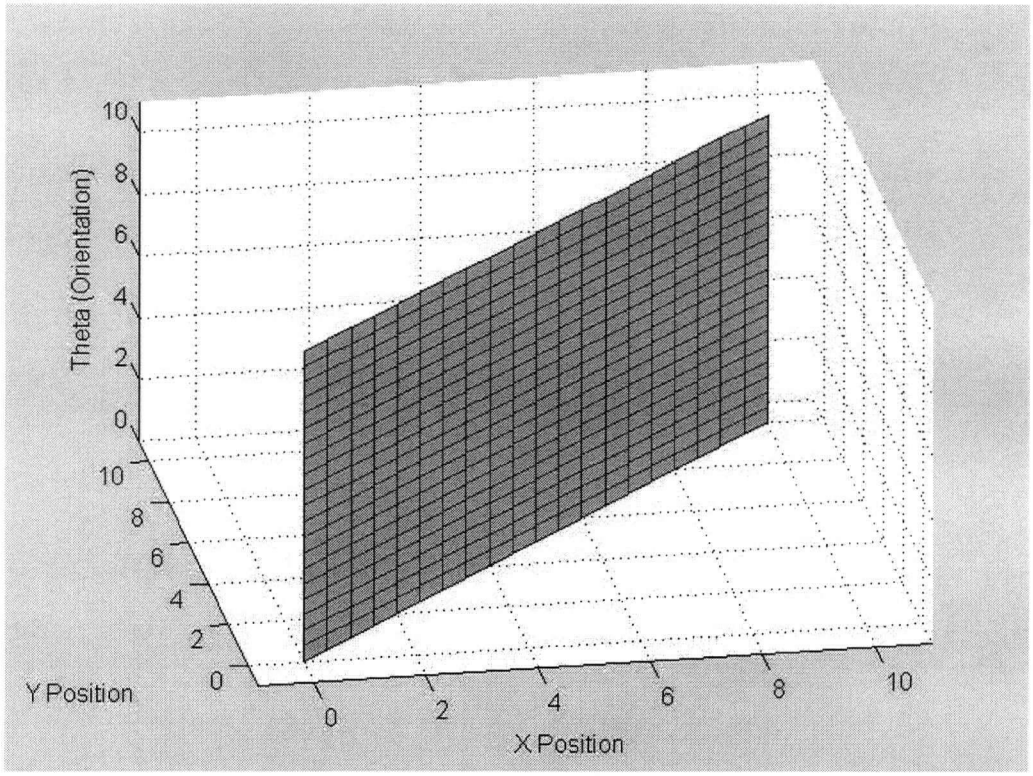

Figure 26. Example of Cart Target Manifold

2.4 Normalization of Taskspace

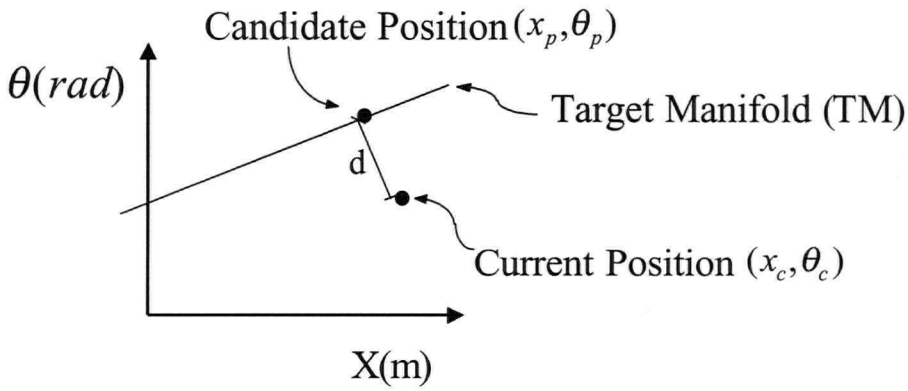

Figure 27. Distance measure in a mixed metric taskspace

The next stage in the controller design is to develop an expression for the distance of the end-effector from the target manifold. Figure 27 shows an example of this distance definition. This task is complicated because the axes in taskspace are in general of mixed units; for example, in our planar cart example, we have two axes with units of length (e.g., *m*) and one with units of angle (e.g., *rad*). We must therefore select an appropriate normalization scheme that will allow us to calculate distances and angles using standard geometric principles. We propose an energy based normalization scheme, which creates a non-dimensional taskspace. To begin we look at displacements in each principle direction, and define the kinetic energy of each using a spring constant. For

example, 'k_x' could be a linear spring constant (N/m) used for displacements along the x axis, and 'k_θ' could be the rotational spring constant (Nm/rad) for displacements along the θ axis. In order to reduce the arbitrariness in selecting values for the spring matrix, we can select spring constants such that the response of an equivalent spring-mass system would have the same natural frequency in both linear and rotational oscillations. The natural frequency would be given by:

$$\omega_n^2 = \frac{k_x}{m} = \frac{k_\theta}{I} \tag{9}$$

Where: m is the mass of the system, and I is the inertia.

If we choose reference displacements such that the energy in the imaginary springs are equal for a one unit displacement in each direction:

$$E = \frac{1}{2}k_x x_0^2 = \frac{1}{2}k_y y_0^2 = \frac{1}{2}k_\theta \theta_0^2 \tag{10}$$

Choosing E = 1 Nm:

$$x_0 = \sqrt{\frac{2}{k_x}} \tag{11}$$

$$y_0 = \sqrt{\frac{2}{k_y}}$$

$$\theta_0 = \sqrt{\frac{2}{k_\theta}}$$

Normalization occurs through the following transformation: (Note: X_{TS} are taskspace coordinates, $\tilde{X}$ are normalized taskspace coordinates)

$$\tilde{X} = \begin{bmatrix} x^{\sim} \\ y^{\sim} \\ \theta^{\sim} \end{bmatrix} = \begin{bmatrix} \frac{1}{x_0} & \frac{1}{y_0} & \frac{1}{\theta_0} \end{bmatrix} X_{TS} \tag{12}$$

Now that we have a transformation to normalized taskspace, all future calculations of distances and angles occur in this space.

2.5 Heading Angle

Having a method of defining the distance from the target manifold through a normalized taskspace, we now design a control law that can steer the end-effector back to the TM in a smooth and controlled manner. Since we can control the differential displacement of the end-effector by changing the steering angles of the CVTs, we need to define an optimal return path to the TM and alter the steering angles to guide the end-effector along this path. By making an analogy to the steering strategy used by most drivers to return their car to the centre of their lane after being displaced from their course, we would suggest that a good return strategy would be to select a path which becomes parallel to the target manifold as we approach it and which begins with a comparatively steeper approach angle when we begin the return maneuver and are still far from the target manifold. Furthermore, to ensure that the resulting motions are smooth and controlled, we should change the steering angles at a moderate rate (rather than "yanking on the wheel"). We formalize this strategy below.

Figure 28 gives a 2D example of how we calculate a heading angle. The heading angle is calculated as the angle between the current velocity vector and a normal to the TM. The reference heading angle is calculated based on

the distance from the TM. Far away from the TM, our reference heading angle will likely be at a minimum, while configurations close to the TM will be progressively more parallel to it.

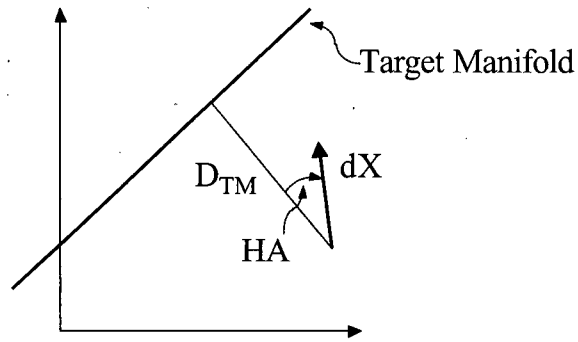

Figure 28. Heading Angle Measurement Example

We now want to define a reference heading angle for the cart. We chose an energy based 'distance' method to determine heading angles at each position. Note: HA is the calculated reference heading angle for the current position; HA_{min} is the minimum allowable approach angle to the target manifold, where 0 is perpendicular to the TM; D_{TM} is the distance to the TM from the current position; and D_{ref} is the reference distance, below which the reference heading angle linearly approaches being parallel to the TM.

$$HA = HA_{\min} + (90 - HA_{\min}) \cdot \left(1 - \min\left(1, \frac{D_{TM}}{D_{ref}}\right)\right) \tag{13}$$

2.6 Coupling Space

Having chosen a reference return path, we are left with the task of selecting the appropriate steering angles and rates of change to achieve it. We begin by considering how the CVTs can affect the motion of the end-effector.

The coupling spaces are used to represent the relationships between differential changes in configuration space variables that the CVTs establish. As a result, the number of coupling spaces is equal to the number of CVTs. Each constraint, α, plus its first derivative, $\dot{\alpha}$, determines the direction and curvature of the cobot path in the associated coupling space.

As an example, a wheel on a cart is a form of CVT. The coupling space for the wheel is shown in Figure 29.

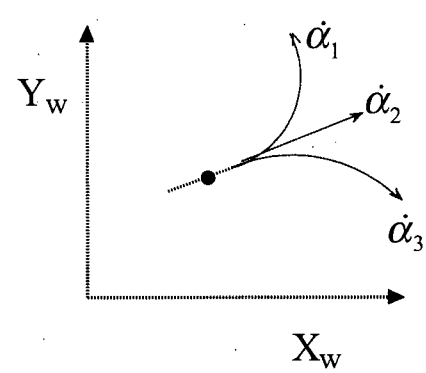

Figure 29. Example of coupling space for a wheel

By controlling $\dot{\alpha}$, the future evolution of the constraint α is achieved. The cobot is then steered through the taskspace according to the constraint changes.

A mapping from normalized taskspace to coupling space is given by:

$$C = F(X^{\sim}) \tag{14}$$

where F maps the normalized taskspace position, $X^{\sim}$, into a coupling space position, C. Differentially, we can express this equation as:

$$dC = J_c(X^{\sim})dX^{\sim} \tag{15}$$

where $dX^{\sim}$ represents a differential displacement in normalized taskspace, dC represents the corresponding mapping into coupling space, and $J_c(x^{\sim})$ is the jacobian matrix. In our cart example, Jc is a 2 x 3 matrix.

Certain components of $dX^{\sim}$ do not project into the coupling space, and are represented by the vector $dXn^{\sim}$. We can solve for $dXn^{\sim}$ by calculating the null space of J_c., which is defined by the set of vectors V which satisfy

$$dC = J_c(X^{\sim})V = 0 \tag{16}$$

We can construct a basis for J_c's nullspace using standard linear algebra tools and represent this basis in the form of a matrix Jn, whose columns are unit orthonormal vectors spanning the nullspace.

$$J_n = [V_1 \quad V_2 \quad \cdots] \tag{17}$$

In our cart example, Jc has a one dimensional nullspace (the dimension of the nullspace is equal to the dimension of the taskspace minus two – the dimension of the coupling space). As a further example, a CVT in a 6 DOF cobot would have a four dimensional nullspace and would therefore be represented by $V_1 - V_4$.

The implication of the existence of a nullspace is that we cannot affect any component of end-effector motion that lies in the nullspace through changes in the steering angles of our CVTs. That is, if the user is maneuvering the end-effector completely in the nullspace, the controller is powerless to resist this motion, even if it is taking the end-effector away from the target manifold. However, if there is a component of motion that lies outside the nullspace, we are able to affect the end-effector motion. Let the portion of $dX^{\sim}$ we can control be represented by $dXc^{\sim}$. This vector lies in a space orthogonal to J_c's nullspace. We compute it simply by finding a basis for all vectors W which satisfy:

$$J_n{}'W = 0 \tag{18}$$

This basis will consist of two vectors in normalized taskspace which span the subspace which has a nonzero projection into the coupling space. We can therefore represent $dXc^{\sim}$ by a linear combination of the bases for the non-null space of J_c.

$$dXc^{\sim} = [W_1 \quad W_2]\begin{bmatrix} a_1 \\ a_2 \end{bmatrix} \tag{19}$$

2.7 Steering Angle

Now that we have a desired heading angle, and a description for the coupling spaces, we set up an optimization problem to find the steering angle that steers the cart velocity closest to the desired HA.

This is accomplished by proposing changes to the steering angle ($d\alpha$) and calculating the new dC component. When calculating the proposed controllable component of the velocity it is important to preserve kinetic energy (KE), since this is normally undisturbed during steering of the cobot. We preserve KE by calculating a factor that scales the new component of velocity appropriately. The controllable component of differential displacement in normalized taskspace, $dXc^{\sim}$, is calculated from dC as follows: (Note k is a constant added to preserve kinetic energy from the original differential displacement).

$$dXc_{new}^{\sim} = kJ_c[W_1 \quad W_2]dA \tag{20}$$

Where:

$$dA = J_w^{-1} dC_{new} \tag{21}$$

Our proposed new velocity vector, $dX^{\sim}_{new}$, is composed of the new $dXc^{\sim}_{new}$ and $dXn^{\sim}$. The heading angle is now calculated as the angle between $dX^{\sim}_{new}$ and the projection of $dX^{\sim}_{new}$ onto the TM.

2.8 Cobotic Control of a Planar Cart

To gain a better practical understanding of the concepts presented, we will illustrate with a few examples. Three situations are presented which show the heading angle determination and generally controllability implications. In each example, a view of both normalized taskspace and coupling space are presented. Our examples are all of a single wheeled cart moving in a 3-dimensional taskspace. The first example presents a straightforward application of the concepts. The second example gives a situation that is problematic from the controller standpoint. The third example is a combination of the first two situations, and allows us to explore potential limitations and problems with minimally constrained cobots.

2.8.1 Example of steering angle determination for Planar Cart

For this example, we will define the TM as being x = 0, with arbitrary rotation. The cart will have $L_x = 0$, which means that the point we are trying to control and the steering wheel are coincident on the cart. Figure 30 shows an arbitrary non-zero velocity and the corresponding $dXc^{\sim}$ and $dXn^{\sim}$ components.

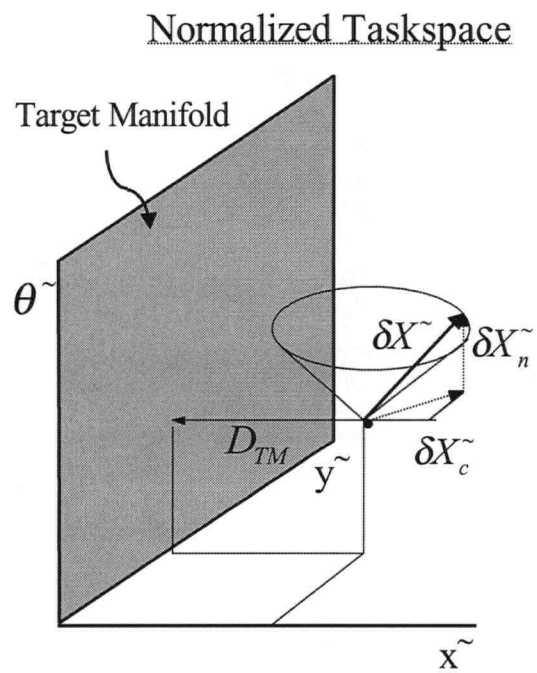

Figure 30. Breakdown of dX into Components for Planar Cobotic Cart

By mapping $dX^{\sim}$ into the coupling space, and changing dC by a steering value $d\alpha$, we create $dC^{\sim}_{new}$.

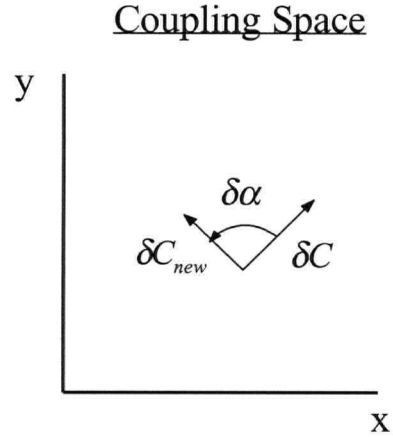

Figure 31. Proposed $d\alpha$ and the corresponding change to dC

Back in normalized taskspace, the resulting $dXc^{\sim}_{new}$ creates a new direction for the differential displacement of the cart which we can then use to compare to our calculated reference heading angle. In effect, changing α allows us to swing $dXc^{\sim}$ around $dXn^{\sim}$, and create a cone of possible new velocities. At most two of these proposed velocities will match the desired heading angle. Once the correct $d\alpha$ is found, we have a quantitative measure of the error in our system, which can be used in a simple PD controller to controller the steering velocity of our wheel motors.

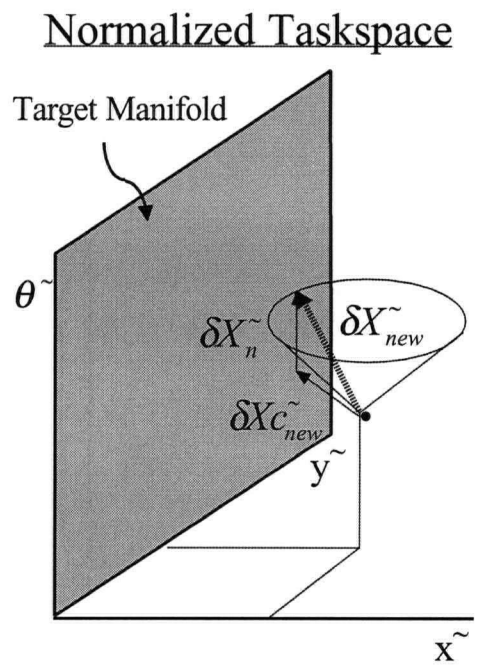

Figure 32. New dX vector based on new steering angle

2.8.2 Planar Cart with Maximized Controllability

As we saw in the previous example, the nullspace component of the cart velocity is parallel to the target manifold. When the cart is in a position away from the TM, we can find a $dXc^{\sim}$ component that matches our

reference heading angle and steer the cart back to the TM. Controllability is at its worst when we have velocities that are entirely defined by the null space of our cobot ($dX^{\sim} = dXn^{\sim}$). In this case, changing the steering wheel does not effect our velocity. In Figure 33, we see the case where we are at a position on the TM with a velocity defined solely by the nullspace of the cart. Since $dX^{\sim}$ is parallel to the TM, even though we cannot steer the cart, the cart will differentially remain on the manifold. Physically, a velocity defined solely by the nullspace would be the cart spinning about the contact point of the wheel with the ground. No amount of steering the wheel will affect the velocity if the cart is only spinning about this contact point.

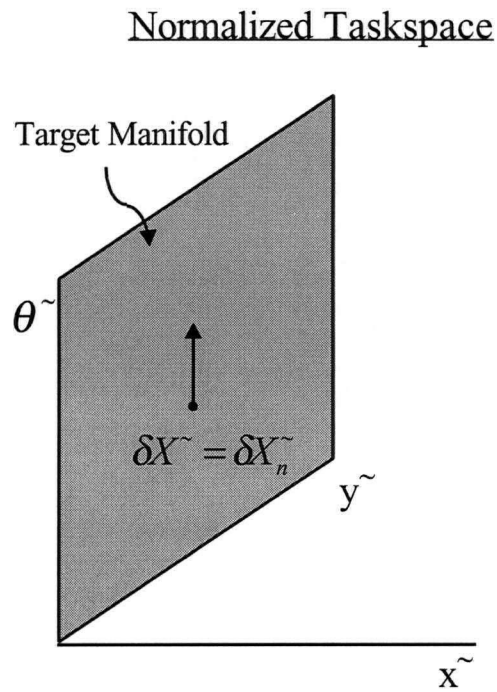

Figure 33. dXn motions on TM

If our position were at some point not on the TM, we would have no recourse but to wait until the user's motion had a $dXc^{\sim}$ component sufficient to steer back to the TM.

2.8.3 Planar Cart with Partial Controllability

Consider a TM that is no longer the y-θ plane, but rather some angled plane in taskspace. If the cart design remains the same we are left with a cart that is controllable only under certain circumstances. For instance, take Figure 34 for example. In this case the cart is moving away from the TM, but we can see that for a certain steering angle, we can achieve a velocity close to the TM.

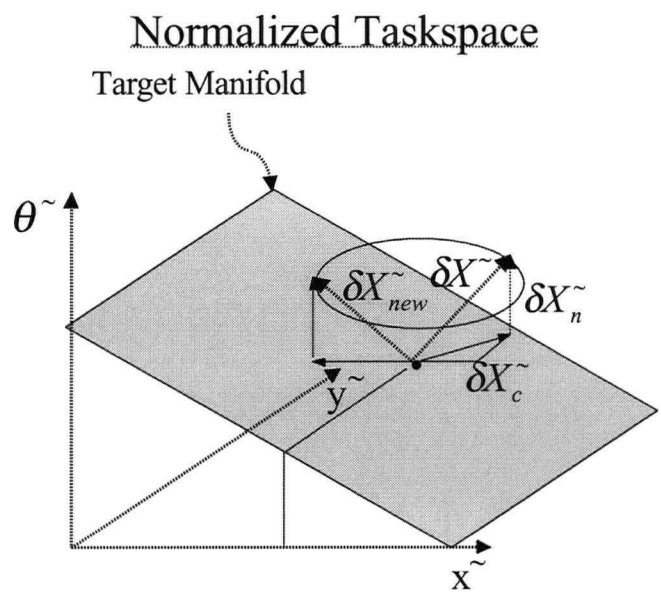

Figure 34. Example of a marginally controllable motion

The extreme case, where the velocity is defined solely by the dXn~ component is shown in Figure 35. Here, we have a case where the cart is moving away from the TM, and we have no way of steering it back to the TM.

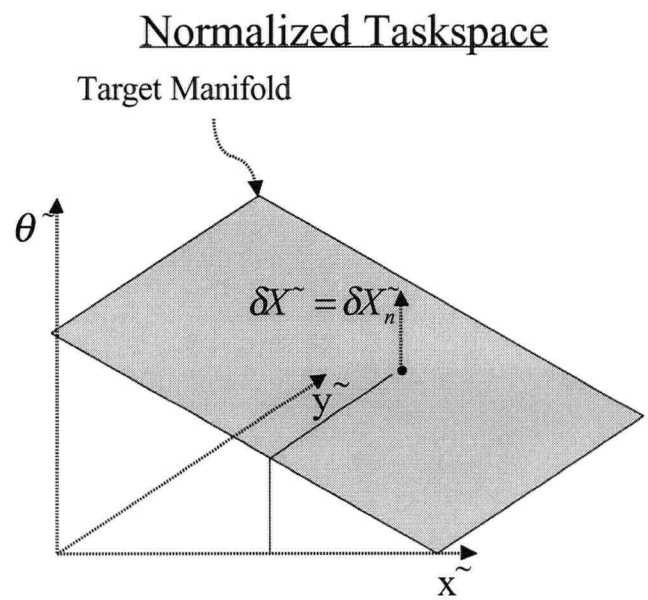

Figure 35. Example of an unacceptable uncontrolled motion

The first example here shows marginally controllability of the cart, while the second example shows the loss of cart controllability. As dXn~ is oriented progressively perpendicular to the TM, there is an increased chance that the user motions will be uncontrollable.

2.8.4 Planar Cart with Minimal Controllability

In this last example, the TM is the x-y plane passing through the origin, as can be seen in Figure 36. Here we have a case where motions in the TM are cause purely by uncontrolled means since the user is capable of moving away from the target manifold in every incident.

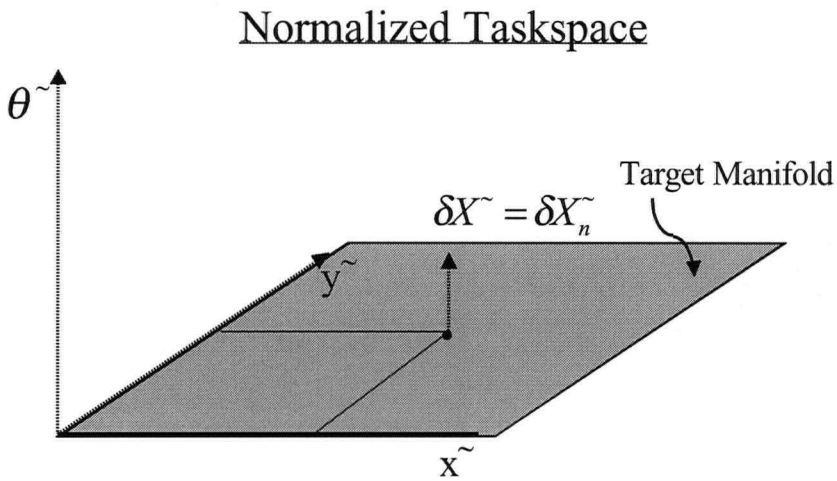

Figure 36. Complete uncontrollable cart configuration

2.8.5 Cart Controllability Summary

From these examples, we can see that it is crucial to ensure that the null-space of the cart is oriented parallel to the TM throughout the workspace.

3.0 Simulation of Cart Motions

A simulation of the cart moving gives us sense of how the controller performs under real conditions.

3.1 Formulation of Lagrangian Equations of Motion

Using Lagrangian equations of motion, the cart is constrained to move under the control of the steered wheel. The formulation of these equations is briefly outlined. First of all, the energy equation is written, which consists of kinetic energy only.

$$L = T^* - V = \frac{1}{2}(m\bar{v}^2 + I\bar{\omega}^2) \tag{22}$$

$$\frac{\partial L}{\partial \dot{q}} = \begin{bmatrix} mv_x \\ mv_y \\ I\omega \end{bmatrix} \tag{23}$$

$$\frac{d}{dt}\frac{\partial L}{\partial \dot{q}} = \begin{bmatrix} m\ddot{x} \\ m\ddot{y} \\ m\ddot{\theta} \end{bmatrix} \tag{24}$$

$$\frac{d}{dt}\frac{\partial L}{\partial \dot{q}_i} - \frac{\partial L}{\partial q_i} = \sum_j \lambda_i a_{ji} + F \tag{25}$$

$$m\ddot{x} = F_x + \lambda \sin(\beta) \tag{26}$$

$$m\ddot{y} = F_y - \lambda \cos(\beta) \tag{27}$$

$$I\ddot{\theta} = \tau - \lambda L(\sin(\theta)\sin(\beta) + \cos(\theta)\cos(\beta)) \tag{28}$$

By differentiating the constraint equation for the cart, we can write a set of equations that can be solved for the cart acceleration.

$$\begin{bmatrix} m & 0 & 0 & -\sin(\beta) \\ 0 & m & 0 & \cos(\beta) \\ 0 & 0 & I & LQ \\ \sin(\beta) & -\cos(\beta) & -LQ & 0 \end{bmatrix} \begin{bmatrix} \ddot{x} \\ \ddot{y} \\ \ddot{\theta} \\ \lambda \end{bmatrix} = \begin{bmatrix} F_x \\ F_y \\ \tau \\ R \end{bmatrix} \tag{29}$$

Where:

$$Q = (\sin(\theta)\sin(\beta) + \cos(\theta)\cos(\beta)) \tag{30}$$

$$R = L\dot{\theta}\dot{\alpha}(\sin(\theta)\cos(\beta) + \sin(\beta)\cos(\theta)) - (\dot{\theta} + \dot{\alpha})(\cos(\beta)\dot{x} + \sin(\beta)\dot{y}) \tag{31}$$

3.2 Implementation of Simulation

The cart simulation is implemented using MATLAB 5.3.[6] The accelerations of the cart (see Equation 29) are solved using MATLAB's 'ode23' solver at each time step during the simulation. The simulation works by taking an initial state vector, retrieving the user input (x-y forces and torque), calling the wheel controller function, and returning the new state vector.

At each time interval, we use an Nelder-Mead optimization in Matlab to determine a new alpha value that best matches that steers the velocity closest to the desired heading angle. Our search starts at $\delta\alpha=0$ (no change to steering angle) and continues until we find a minimum between the proposed and desired heading angle.

The calculation of the steering velocity is shown in Figure 37.

[6] See Appendix E for the organization of the MATLAB code

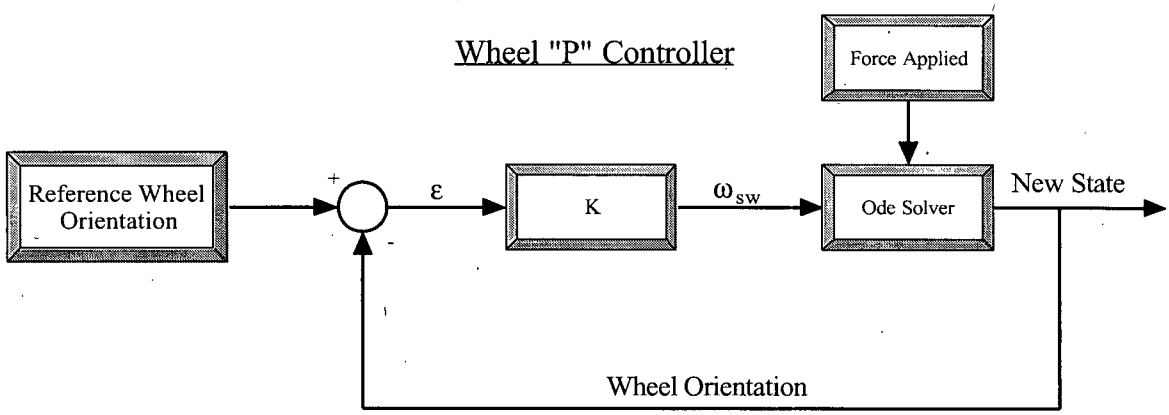

Figure 37. Control Diagram for Cart Steering Wheel

An acceptable proportional gain of k=5 was chosen through inspection and iteration, however the value is likely not optimal. In addition to optimizing the proportional gain, a derivative component should be added to the controller. It was not included in this simulation because of limitations in the Matlab environment.

3.2.1 User Input

Since the motive forces for the cobot are coming from the user applying force, we need to create a method of calculating applied force in a way that has some rationale. Since the forces exerted by the user are, to some degree, position dependent, we use a virtual trajectory calculation to derive applied forces and torques. The virtual trajectory defines a reference position and orientation for the user's hand. We can think of this virtual position as being where the user's hand wants to be. The force applied by the user is directly proportional to the distance between the actual cart position, and where the user's hand wants to be at that instant. Because of the proportionality, we can use a spring model to approximate the applied force. Note: F is the calculated applied force; $X_{Virtual}$ is the virtual configuration; $X_{Current}$ is the current configuration; K_F is a vector of linear and rotational spring constants.

$$\overline{F} = (\overline{X}_{Virtual} - \overline{X}_{Current})\overline{K}_F$$

3.2.2 Conditions for Simulation

3.2.2.1 Initial Conditions

The cart used in the simulation has dimensions of 0.5 x 0.3 m and weighs 1kg. The steering wheel is modeled to have no mass. Initially, the cart is standing still at the origin, with $\theta = \alpha = 0$. The simulations are each run for 8 seconds.

In each simulation, two figures are created. The first figure shows the cart position every 0.4 seconds. A black line connects the current and virtual configurations of the cart. A thin blue line represents the direction of the wheel, and the yellow circle denotes the centre of the wheel.

The second figure gives a metric for the distance of the cart's configuration from the target manifold. When the distance metric is 0, the configuration of the cart is exactly on the target manifold. This figure gives an indication of how well the controller is performing under the conditions applied.

3.2.2.2 Force-Torque Input

The force-torque information was synthesized by having a virtual trajectory of the user hand starting at the origin and moving with a velocity of $[v_x, v_y, \omega]$ = [-.1 m/s, 1 m/s, 0.05 rad/s]. Linear spring constants of 0.1 N/m

were chosen for calculating the linear force applied to the cart. Rotation spring constants of 0.1 * mc/I were chosen to keep the natural frequency of both linear and rotational constants the same.

3.3 Simulation Results

3.3.1 Simulation 1

In this simulation, the wheel and control point are coincident, and the TM is a plane at x=0 for any orientation. As discussed, this means that dXn is parallel with the TM throughout the configuration space. Rotations of the cart about the wheel pivot are uncontrolled, but only result in a change in orientation for the control point. At worst this does not allow the cart to converge to the TM, and at best it results in motions that keep the cart on the TM. (See figure 38)

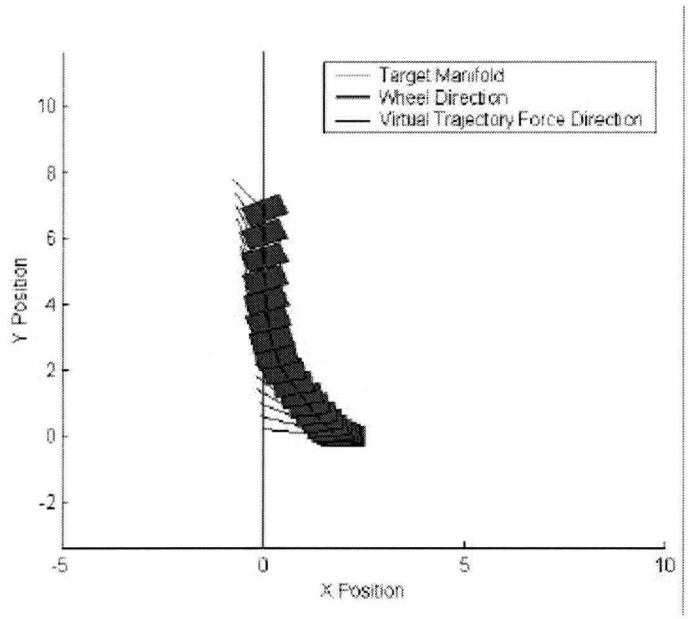

Figure 38. Simulation 1 – Control Point and Wheel Coincident – Top View

Figure 39 gives a good indication of how well the cart is controlled to the target manifold. In this case, the cart approached the TM quickly, and remains there even when applied forces try to pull it off of the TM. For this case, the cart and controller are designed appropriately.

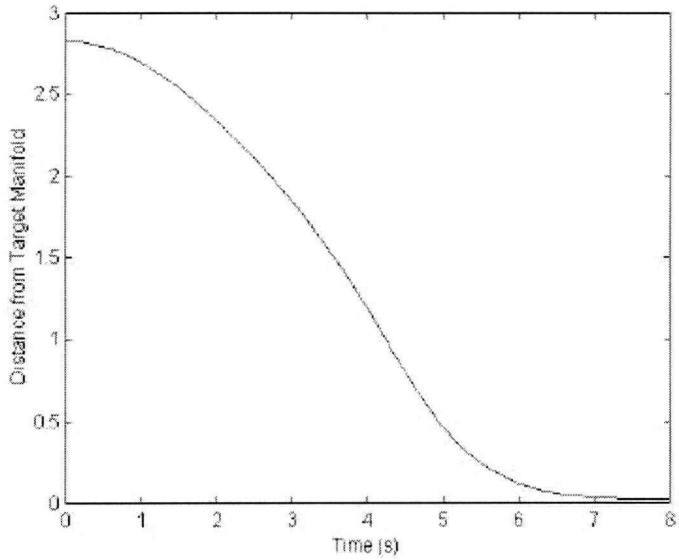

Figure 39. Simulation 1 – Control Point and Wheel Coincident – Distance from TM

3.3.2 Simulation 2

In this second simulation, the wheel is 0.3m away from the control point (lx=0.3) and the TM remains the same plane as in simulation 1. As discussed, dXn is now a function of the cart orientation, and is only parallel to the TM in certain orientations. Since this isn't the ideal cart configuration for the controller we expect to see decreased controller performance. (see Figure 40)

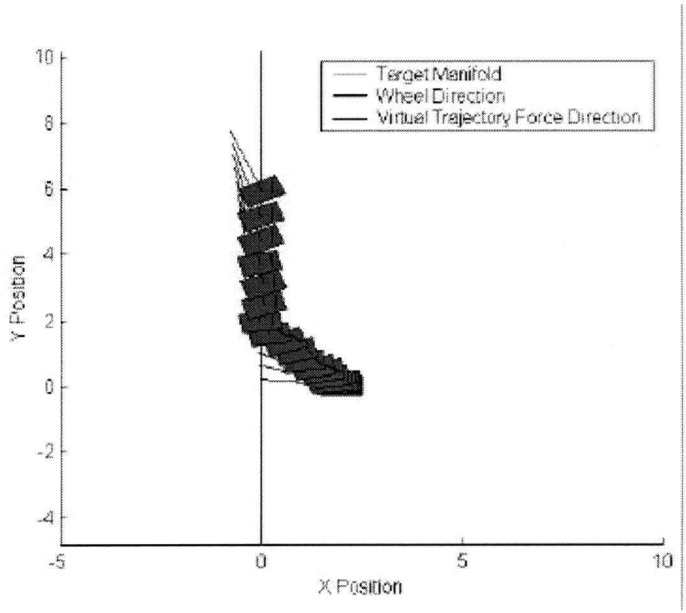

Figure 40. Simulation 2 – Wheel Offset by 0.1m from Control Point – Top View

Figure 41 shows us the controller is still able to control the cart to the TM, however the results also show that the nullspace causes control problems which cause non-ideal results.

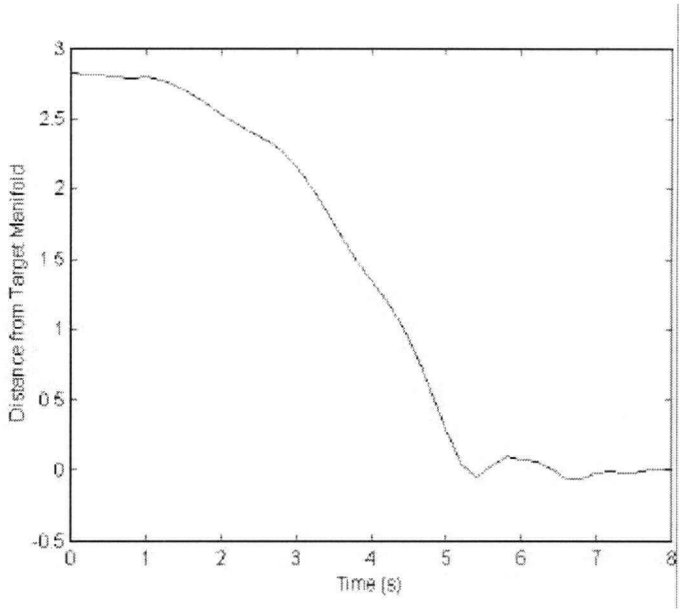

Figure 41. Simulation 2 – Wheel Offset by 0.1m from Control Point – Distance from TM

4.0 Discussion

The theory presented in this paper can be applied to higher dimensional parallel cobots. The most common type of parallel manipulator is the stewart platform, which has 6 legs. This type of manipulator is full constrained when the legs are not changing length, and therefore has a 0 DOF nullspace. We anticipate continuing this research on a 4 legged parallel manipulator for use in guidance tasks in knee surgery (see Figure 44 for a simple example). The objective in knee surgery would be constructing a 3 DOF plane for bone saw motion, in order to accurately define cutting plane. With only 4 legs, a 2 DOF null space is created (dXn). It can be calculated by taking the null of the manipulator jacobian for the parallel platform. A prototype CVT for use with this type of manipulator has already been designed (Emrich, 2000), which would be used to create a 1 DOF dXc space for the manipulator. The result is a platform that is capable of achieving the 3 DOF motion required for the guidance task. The challenge will now be designing the leg positions such that the null space will be nominally parallel with the desired cutting plane throughout the workspace.

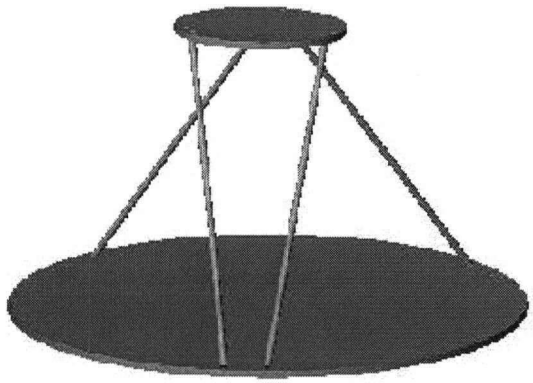

Figure 42. Example of a 4 Legged Parallel Platform Manipulator

In terms of the control structure laid out in this paper, the 4 legged manipulator would have 4 steering spaces (1 for each CVT), 4 coupling spaces, a 6 dimensional taskspace, and a 4 dimensional configuration space. As mentioned, any differential motion of the manipulator, dX, would be composed of some linear combination of dXn (2 dimensional) and dXc (1 dimensional).

From example and simulations shown in this paper, we can see that when dXn is not aligned with the TM, the possibility exists for velocities to be composed of relatively large dXn components and small dXc components. In other words, the motion is uncontrollable because dXc, our steerable component is not large enough to steer the guided object back to the TM. The guided object now drifts off the TM at a rate proportional to the misalignment of dXn with respect to the TM.

The result is clear limitation for creating a 3 DOF TM using a slightly misaligned 2 DOF nullspace. If we know that our task requires motions in all 3 DOF, we can expect that at times, the velocity will be defined largely by nullspace motions, which can result in uncontrolled divergence from the TM. Using our planar cart and the TM presented in the simulations, a cart with $lx \neq 0$ has a dXn misaligned with the TM in certain cart orientations. We can compensate for the errors introduced by this misalignment when the dXc component is sufficiently large to allow steering back to the TM. If our task required us to pivot the cart only about the wheel point, we could fail to adequately constrain the cart to the TM. This approach to a multidimensional TM will only be successful if we know our primary direction of motion will cause velocities to be composed of large dXc components. The result is a system that is best suited to TMs where we expect velocities to be biased towards the dXc direction, instead of allowing motions freely in any direction in the TM.

In terms of the practical implementation of the controller, the controller works, but the proportional gain for the wheel controller is not optimized, and it would be desirable to include a derivative component in future work. Actual implementation will have much to do with the motors chosen for the steering, and their physical characteristics. The code used in the MATLAB simulation worked, but was computationally slow and requires work to decrease run times. A typical 8 second simulation took about 5 minutes on a 450 MHz processor.

In addition, the virtual trajectory force calculation was a good idea, but the virtual trajectory itself was determined before the simulation started. In certain situations, the choice of change in steering direction is arbitrary, and the cart is steered away from where the virtual trajectory is moving. The result is instability in the simulation, since large forces were being exerted perpendicularly to the wheel direction. The cart slows to a stop, and this acts as a type of singularity for the wheel controller since it depends on motion for steering decisions. In reality, if the user felt the system was 'fighting' them, they would probably try a slightly different approach, which our implementation was not capable of simulating. Real time input of user force data from a force transducer would improve the power of the simulation results.

5.0 Conclusions

This paper describes a new direction for cobotic research. We present the concept of minimally constrained design of cobots, and also their application to parallel configurations. This represents a new and exciting direction for research in both cobot design and control. In addition, we believe that this work is a big step towards creating a passive device that has few safety barriers blocking it from being implemented in the operating theatre. We also believe that this device will be capable of improving the longevity of knee prostheses, by increasing the alignment accuracy.

References

Book, W, Charles, R, Davis, H, and Gomes, M. Concept and implementation of a passive trajectory enhancing robot. Proceedings of the ASME Dynamic Systems and Control Division American Society of Mechanical Engineers, Dynamic Systems and Control Division 58, 633-638. 1996. Atlanta, GA. Proceedings of the 1996 ASME International Mechanical Engineering Congress and Exposition. Conference Proceeding

Colgate, JE, Wannasuphoprasit, W, and Peshkin, MA. Cobots: robots for collaboration with human operators. Proceedings of the 1996 ASME International Mechanical Engineering Congress and Exposition 58, 433-439. 1996. Atlanta, GA. Proceedings of the International Mechanical Engineering Congress and Exhibition. Conference Proceeding

Davies, BL, Harris, SJ, Lin, WJ, Hibberd, RD, Middleton, R, and Cobb, JC: Active compliance in robotic surgery--the use of force control as a dynamic constraint. Proceedings of the Institution of Mechanical Engineers, Part H 211:285, 1997.

Emrich, RJ and Hodgson, AJ: A CVT Element for Parallel Cobots. Submitted to ASME Haptic Interfaces for Virtual Environment and Teleoperator Systems, November 2000.

Figgie, HE, Goldberg, VM, Figgie, MP, Inglis, AE, Kelly, M, and Sobel, M: The effect of alignment of the implant on fractures of the patella after condylar total knee arthroplasty. J.Bone Joint Surg.[Am.] 71:1031, 1989.

Gillespie, RB, Colgate, JE, and Peshkin, M: General framework for cobot control. Proceedings IEEE International Conference on Robotics and Automation 3:1824, 1999.

Gomes, MW and Book, WJ. Control approaches for a dissipative passive trajectory enhancing robot. IEEE ASME International Conference on Advanced Intelligent Mechatronics , 92. 1997. IEEE ASME International Conference on Advanced Intelligent MechatronicsBı. Conference Proceeding

Inkpen K.B., Precision and Accuracy in Computer Assisted Total Knee Replacement. Master of Applied Science Thesis, University of British Columbia, December 1999.

Jeffery, RS, Morris, RW, and Denham, RA: Coronal alignment after total knee replacement. J.Bone Joint Surg.[Br.] 73:709, 1991.

Leitner, F, Picard, F, Minfelde, R, Schulz, H-J, Cinquin, P, and Saragaglia, D. Computer Assisted Knee Surgical Total Replacement. Troccaz, J, Grimson, E, and Mosges, R. 629-638. 1997. Grenoble, France, Springer-Verlag. CVRMed - MRCAS Proceedings '97. Conference Proceeding

Moody JE, DiGioia AM, Jaramaz B, Blackwell M, Colgan B, and Nikou C: Gauging Clinical Practice:Surgical Navigation for Total Hip Replacement. Med.Image Computing and Computer-Assisted Int.-MICCAI'98 .Lecture Notes in Comp.Science 1496:421, 1998.

Moore, CA, Peshkin, MA, and Colgate, JE. Design of a 3R cobot using continuously variable transmissions. Proceedings IEEE International Conference on Robotics and Automation 4, 3249-3254. 1999. New York, IEEE. Proceedings of the 1999 IEEE International Conference on Robotics and Automation, ICRA99. Conference Proceeding

Moreland, JR: Mechanisms of failure in total knee arthroplasty. Clin.Orthop. 49, 1988.

Rand, JA and Ilstrup, DM: Survivorship analysis of total knee arthroplasty. Cumulative rates of survival of 9200 total knee arthroplasties. J.Bone Joint Surg.[Am.] 73:397, 1991.

Tonetti, J, Carrat, L, Lavallee, S, Pittet, L, Merloz, P, and Chirossel, JP: Percutaneous iliosacral screw placement using image guided techniques. Clin.Orthop. 103, 1998.

Troccaz, J and Delnondedieu, Y: Semi-active guiding systems in surgery. A two-DOF prototype of the passive arm with dynamic constraints (PADyC). Mechatronics 6:399, 1996.

Wannasuphoprasit, W, Akella, P, Peshkin, M, and Colgate, JE. Cobots: a novel material handling technology. Proceedings of the 1998 ASME International Mechanical Engineering Congress and Exposition , 1-7. 1998. Fairfield, NJ., ASME. Proceedings of the 1998 ASME International Mechanical Engineering Congress and Exposition. Conference Proceeding

Wannasuphoprasit, W, Gillespie, RB, Colgate, JE, and Peshkin, MA. Cobot control. Proceedings IEEE International Conference on Robotics and Automation 4, 3571-3576. 1997. New York, IEEE. Proceedings of the 1997 IEEE International Conference on Robotics and Automation, ICRA. Conference Proceeding

Chapter 5 – Thesis Summary

There is a huge volume of research papers on TKA, covering a wide array of topics. The introduction to this thesis attempts to present a clear picture of the problems facing TKA surgery based on a comprehensive literature review. From this, we can see that TKA is an important procedure that increases the quality of life for many people each year. The relationship between failure rates and frontal plane alignment is significant, although no definitive misalignment tolerance has been proven. This is due in part, to limitations in measurement accuracy, and improper definition of alignment angles, such as anatomical alignment. Conventional alignment jigs, radiographic measurement errors and implementation errors are all major contributors to poor frontal plane alignment in the current TKA technique.

Since soft tissue balancing issues are tough to define and vary from surgeon to surgeon, we chose to focus on methods of increasing the alignment accuracy in TKA. Initial work in this area focused on a more accurate method of defining the mechanical axis of the lower limb. Kevin Inkpen, Antony Hodgson and I wrote a paper for MICCAI '98 that detailed a probe design that could more robustly locate exposed, rounded, anatomical features, such as the femoral condyles. Through simulations, we found that point probes were susceptible to deviations in the surface of the joint; a common occurrence in patients with osteoarthritis. We presented two other probe designs that contact the joint using flat probe surfaces, and provide a more robust location of the centre of these nominally round joints.

Through this initial work, two main paths were identified for improving alignment accuracy. The first was continuing the work for a more accurate method of identifying the mechanical axis of the lower limb, and better cutting guide placement. Kevin Inkpen conducted this research as part of his Masters thesis. The second path addresses surgical implementation errors, such as skewing and improper seating of the bone saw on the cutting guides. I chose to pursue this path for my Master's research.

Cobots are capable of increasing the overall accuracy of the procedure, both through incorporating improved mechanical axis determination, and increased implementation accuracy. Systems with the potential to increase the implementation accuracy have historically had problems being adopted in the operating theatre because of safety concerns. A number of groups have technology capable of providing passive guidance of tools, thereby eliminating limiting safety concerns. Most of these systems are designed to enforce 'zones of exclusion', but are not well suited to the creation of smooth, planes of motion, which would be necessary in TKA. Cobots, on the other hand can create smooth programmable, virtual constraints, and are inherently passive devices.

Currently, cobots are implemented using transmissions that relate rotational velocities. This has resulted in a serial and parallelogram cobot. The parallelogram cobots cannot be extrapolated to high enough dimensions to be useful in knee surgery and serial manipulators, although well suited for many industrial operations, are far less accurate when compared with parallel manipulators. In addition parallel manipulators are capable of far lighter configurations, thereby increasing manoeuvrability, since drive mechanisms can remain stationary in the platform base. A parallel cobot would provide an ideal solution for increasing the accuracy of TKA, with passive tool guidance.

Parallel manipulators are controlled by changing the length of the support legs. The rotational CVTs that exist are not suitable for parallel cobots, since the legs require changes in length, rather than orientation. Chapter 3 presents our work on the first CVT element for use with prismatic legs. The concept was fleshed out by crude wood prototype, and a more sophisticated final aluminium prototype. This work involved 3D modeling of the seating device (used to keep the leg link attached to the drive mechanism); friction calculations for sizing the steering motor; selecting and purchasing of a motor; creating a brace to protect the motor from seating forces; and selecting and purchasing all necessary bearings.

A control architecture was also developed to steer the CVTs of the manipulator. A major component of this system was the interface card which communicates between the computer and the motors. Our initial work was plagued for months by errors in third party software, and we eventually purchased a new board capable of communicating directly the controller. The controller is implemented in real time through Matlab's Real Time Workshop, and first order controller function was verified through custom position control code. A fan cooled

control box was built, which houses a power supply and all the motor controllers. Wiring, and all connections were also designed and built to link the computer, motors, and position feedback encoders.

Cobots are currently implemented as 0 or 1DOF devices. They are capable of creating 1 direction of motion at a time. Higher dimensional motions are simulated using force sensing and selective alignment of the CVTs. This requires high speed control of the CVTs in order to avoid a course feel. In addition, force sensing introduces a time lag that contributes to potential unstable control oscillations. Because TKA requires motions to be controlled to a 3 dimensional space, we wished to develop a method that could provide sufficient constraint for the task, while avoiding the need for selective alignment of constraints. We introduce the concept of minimally constrained cobots design, which allows the manipulator to moving with the same degrees of freedom as the desired control space.

Although our objective is to create a controller, and a 6 DOF parallel platform for surgical tool guidance, we present the groundwork for the controller using a lower DOF device. By taking this step, important concepts, like the nullspace, and the controllable space can be shown easily using 3 dimensional graphs, as opposed to presenting 6 dimensional data.

We also detail concepts important to controllability of minimally constrained cobots. For instance, we show that it is crucial to properly design the nullspace of a cobot with respect to the TM.

In sum, this thesis creates the groundwork for a new passive manipulator for surgical applications. I present the first CVT suitable for parallel platforms, and discuss the formulation of the manipulator Jacobian for a device with variable leg-base attachments. I also introduce for the first time, the concept of a minimally constrained parallel cobot. A controller suitable for minimally constrained cobots is developed, and examples, as well as simulations, are presented for a planar cart.

Future Work

The prototype CVT built is an invaluable tool for learning how to create the final CVT design for a parallel cobot. Research is needed to provide a maximum end effector force that can be sustained by the CVT, and to determine the efficiency of the drive mechanism. The current design has a limited range of motion, which may be optimized in the next design iteration. The orientation of the CVT with respect to the base of the platform, may be required to create sufficient end effector range of motion. Lastly, a method of coupling all the transmissions need to be addressed.

Future work on the control architecture will being by implementing a control architecture using Matlab's Real Time Workshop. Coding needs to be completed to integrate information from optoelectronic devices necessary for the calculation of correct cutting planes). Concepts such as coupling spaces and null spaces need to be extrapolated and coded into Real Time Workshop for the parallel platform.

We have identified factors contributing to maximized controllability of cobots. The design of a minimally constrained parallel cobot for TKA will require careful definition of the necessary workspace, and design of a manipulator with maximized controllability throughout this space. Scaling of the platform, and the CVTs will also be required.

Appendix A - Rotational Alignment in TKA

1.0 Rotational Alignment

1.1 Importance of Rotational Alignment

Rotational alignment was recently identified as another important factor in knee function.(Berger 1993; Moreland 1988; Rhoads 1993; Stiehl 1996) Malrotation causes abnormal articulation of the knee joint as well as improper patellar tracking. Clinically, this is seen as anterior knee pain, increased patellar component wear, clicking of the knee during articulation, and increased chance of patellar fractures. There is evidence to suggest that external rotation of the femoral component provides improved knee function.(Anouchi 1993) The study examined four cadaver knees and concluded that external rotation provided varus-valgus stability closest to a normal knee; allows proper patellar tracking; and more evenly distributes contact at the patellofemoral joint between the femoral condyles.

Anouchi identifies 5° external rotation of the femoral component as giving the best patellar tracking and most normal distribution of patellofemoral contact.(Anouchi 1993) There are other studies detailing the benefits of external rotation of the femoral component on patellar tracking and forces(Rhoads 1993), although one other study (Rhoads 1990)says that rotational effects have little influence over patellofemoral forces and that more work needs to be done to determine the correct angular alignment.(Zhang 1996)

Tibial alignment has best rotational alignment when in neutral to slightly externally rotated with respect to the femoral component.(Eckhoff 1997) Increased tibial external rotation has been identified as a factor contributing to anterior knee pain.

1.2 Methods of Implementing Femoral Rotational Alignment

The rotation of the femoral component in most alignment systems is set by attempting to resect the same amount of bone off of the posterior condyles of the femur.(Moreland 1988) This method involves 'eyeing-up' the original condyles, and resecting similar amounts off each condyle. The method has obvious approximation errors and does not apply for some cases where ligamentous imbalance occurs.

A few newer studies suggest that using the posterior condyle for reference is inaccurate and can be improved by using the anteroposterior axis.(Whiteside 1995) This technique uses a line which passes through the deepest part of the patellar grove anteriorly and the intercondylar notch posteriorly. Unfortunately, the only other study concluded that the anteroposterior axis induces excessive external rotation of the femoral component and is difficult to locate during surgery.(Poilvache 1996)

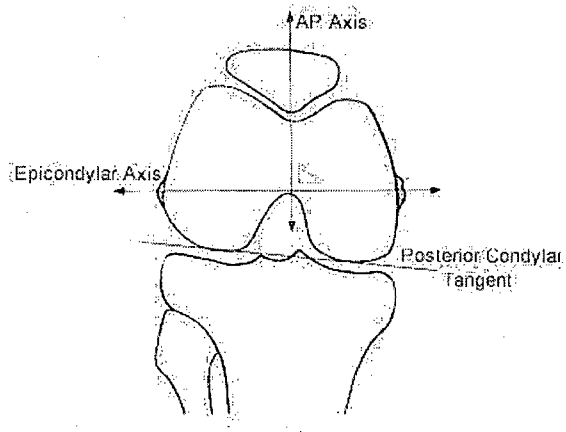

Transverse femur with reference points

The transepicondylar axis is also used as a rotational alignment landmark. It is defined by the axis passing through the two epicondylar peaks when the distal end of the bone is examined, as shown in Figure 6. It produces a more reliable femoral component rotation than the anteroposterior alignment technique(Poilvache 1996; Stiehl 1996), but is tougher to locate intraoperatively.(Whiteside 1995)

1.3 Methods of Implementing Tibial Rotational Alignment

Tibial rotational alignment usually involves using a tibial component that slides over the resected bone. When the tibia is moved through a range of motions, the component moves naturally into the correct orientation. The hope is that the tibial component settles into a position which experiences reduced mechanical stresses through knee motion.

A study of rotational alignment accuracy looked at the relative rotation of the tibial component relative to the femoral component.(Eckhoff 1995a). Four of the techniques use anatomic references such as the tibial tubercle, the posterior tibial axis, the transtibial axis and the malleolar axis. The last two techniques are the range of motion (ROM) method and a method coupling the tibial component to the femoral component using a tensor jig. The tensor jig is a device placed in between the tibia and the femur to achieve soft tissue balance. By placing the knee in flexion and effectively creating a gap between the femur and tibia, the ligaments are stretched and an indication of correct alignment can be achieved.

The four anatomic reference methods rely on a false assumption that anatomic landmarks have a fixed relationship relative to each other in all individuals.(Eckhoff 1994) Surprisingly, the ROM technique also proved to be one of the least reliable techniques although it is still favoured in the O.R.. (Moreland 1988)

The coupled component technique provided the most reproducible alignment, (2° +/- 2° internal rotation) however the definition of correct rotational alignment of the tibia is still not clear.

1.4 Postoperative Assessment of Rotational Alignment

Postoperatively, alignment can be measured with particular prostheses. One method uses one lateral radiograph of the knee in full extension.(Eckhoff 1995b) Once again radiographic technique is identified as being crucial.(Eckhoff 1994) It is limited to femoral component anchored with pegs and still requires clinical correlation of the technique.

Reference List

Anouchi, YS, Whiteside, LA, Kaiser, AD, and Milliano, MT: The effects of axial rotational alignment of the femoral component on knee stability and patellar tracking in total knee arthroplasty demonstrated on autopsy specimens. Clin.Orthop. 170, 1993.

Berger, RA, Rubash, HE, Seel, MJ, Thompson, WH, and Crossett, LS: Determining the rotational alignment of the femoral component in total knee arthroplasty using the epicondylar axis. Clin.Orthop. 40, 1993.

Eckhoff, DG: Effect of limb malrotation on malalignment and osteoarthritis. Orthop.Clin.North Am. 25:405, 1994.

Eckhoff, DG, Brown, AW, Kilcoyne, RF, and Stamm, ER: Knee version associated with anterior knee pain. Clin.Orthop. 152, 1997.

Eckhoff, DG, Johnston, RJ, Stamm, ER, Kilcoyne, RF, and Wiedel, JD: Version of the osteoarthritic knee. J.Arthroplasty 9:73, 1994.

Eckhoff, DG, Metzger, RG, and Vandewalle, MV: Malrotation associated with implant alignment technique in total knee arthroplasty. Clin.Orthop. 28, 1995a.

Eckhoff, DG, Piatt, BE, Gnadinger, CA, and Blaschke, RC: Assessing rotational alignment in total knee arthroplasty. Clin.Orthop. 176, 1995b.

Moreland, JR: Mechanisms of failure in total knee arthroplasty. Clin.Orthop. 49, 1988.

Poilvache, PL, Insall, JN, Scuderi, GR, and Font-Rodriguez, DE: Rotational landmarks and sizing of the distal femur in total knee arthroplasty. Clin.Orthop. 35, 1996.

Rhoads, DD, Noble, PC, Reuben, JD, Mahoney, OM, and Tullos, HS: The effect of femoral component position on patellar tracking after total knee arthroplasty. Clin.Orthop. 43, 1990.

Rhoads, DD, Noble, PC, Reuben, JD, and Tullos, HS: The effect of femoral component position on the kinematics of total knee arthroplasty. Clin.Orthop. 122, 1993.

Stiehl, JB and Cherveny, PM: Femoral rotational alignment using the tibial shaft axis in total knee arthroplasty. Clin.Orthop. 47, 1996.

Whiteside, LA and Arima, J: The anteroposterior axis for femoral rotational alignment in valgus total knee arthroplasty. Clin.Orthop. 168, 1995.

Zhang, AX, Miller, MC, Berger, RA, Sherwood, CP, Petrella, AJ, and Rubash, HE: Effect of Component Placement on the Patellofemoral Joint after Total Knee Arthroplasty. Advances in Bioengineering 33:451, 1996.

Appendix B - Safety Issues in Computer Assisted Surgery

1.0 Safety Problems in CAS

Besides the reliance of most systems on expensive and radiation intensive CT scanning, safety conerns are the single biggest reason for the lack of wide spread adoption of CAS for orthopaedic procedures, especially TKA. Of the systems discussed, only PADyC and P-TER are passive systems that avoid the brunt of safety scrutiny.

1.1 Traditional Robotic Safety

In the past, safety applied to human-robot interaction was limited to Traditional applications of safety to robotic systems have included preventing humans from entering the workspace of the robot. Unfortunately, in a surgical setting the very nature of work involves humans being in the robot's workspace. Because of this need, there have been attempts to define the characteristics of a 'safe' medical robot.

1.2 ROBODOC™ Safety Issues

In the ROBODOC™, a dedicated safety processor ensures that operating tolerances are not exceeded. [8] Some examples are forces at the end effector, bone motion and changes in the arm position. It also checks to ensure proper signals are passed to the cutter and that the Emergency Power Off signal is functioning. The position and motions of the robot are verified by the control computer and by independent encoders. A passive 3 DOF robot monitors bone motion during surgery to reduce potential milling errors. All redundant systems must be satisfied before milling can take place.

1.3 Problems with Modified Industrial Robots

Bouazza-Marouf et al. even go so far as to say that merely modifying industrial robots will not provide an optimum surgical robot.[9] The high cost of modifications and inherent safety issues make it unlikely that such a robot would be adopted in a surgical setting. This is juxtaposed with the apparent success of ROBODOC in a limited hip milling setting.

2.0 Requirements of CAS systems

Stulberg and Kienzle III summarised five requirements of an effective CAS system.[1] Safety for the patient and surgeon must be paramount because of the intimate contact with humans. The system must have sufficient accuracy for the task at hand, including such things as registration in the actual surgery. The system must be able to be made sterile for the procedure. Design of the system should include ergonomic considerations to minimise complexity of the operating room environment and increase ease of use. Lastly, in addition to improved outcome of the procedure, some measurable benefit over existing methods must be quantified, such as time savings or cost savings.

Appendix C - Supplemental Information on Imaging Techniques

1.0 Imaging Techniques

1.1 Roentgen Stereophotogrammetry

Roentgen stereophotogrammetry is a technique involving the precise determination of the location of implanted spherical balls and results in knowledge of relative motion of the balls. This technique is predominantly used in kinematic analysis of orthopaedic components to determine movement of the implants over time and determination of bone growth.(Selvik 1989; Kiss 1995; Ryd 1993). One of the reasons it is favoured is for its high accuracy and use of the commonly available x-ray machine. This procedure requires the implantation of tiny tantalum balls during a procedure and the subsequent analysis of the motion of these markers relative to each other or other landmarks such as a prosthetic component over time. Until recently, it was manually intensive to locate all of the balls for digitization. This process has recently been automated using digital image processing techniques.(Wang 1996) Another drawback of this system is the need for an extensive calibration procedure.(Selvik 1989)

The process is able to determine accurately the 3D location of the balls, but unless they are implanted relative to known landmarks of the body, it would be useless to determine their locations. This method creates points in the body that are easy to find on radiographs, as opposed to anatomical landmarks which are easily obscured. In studies of kinematics and especially bone growth, the location of the balls relative to other landmarks is not as crucial, as relative motion is important. This is in direct contrast to orthopaedic procedures. In computer assisted surgery, the exact location of anatomical reference points is necessary. The additional trauma of implanting the balls and effort needed to figure out how they relate to points of interest make this method impractical for TKA surgery in its current form.

1.2 Fluoroscopy

Fluoroscopy uses a florescent coating on a glass slide to capture the image of x-rays passing through the body. This system has also been used to plan orthopaedic procedures.(Santos-Munne 1996) Two roughly orthogonal fluoroscopic images are taken using a C-arm fluoroscope. The images are not combined, but rather a point or trajectory is specified by identification on the two images. When the procedure is executed, the computer image is used to plan the path of a robot which positions a drill guide. This system must be used intraoperatively and no pre-planning can be undertaken. One of the major benefits of this system, is the use of readily available fluoroscope equipment. This simplification reduces the cost of the procedure and increases ease of execution. The monitors and computer hardware used are complicated, but comparable to CT-scan planning equipment.

1.3 CT-Scanning

CT-scans can also be used to plan trajectories and procedures for orthopaedic surgery. This method constructs a 3D model of the anatomy and allows for the planning of a procedure in advance. It also requires tricky image processing problems such as edge detection and filtering necessary for a clear and accurate image. As well, the 3D model loses subtleties such as brightness, which is present in x-ray images. CT equipment is also less available than x-ray equipment and far more costly. The exposure to radiation is two orders of magnitude higher than receiving a convensional radiograph. On the positive side, they avoid parallax and lens distortion errors, which occur with all of the x-ray imaging devices.

Reference List

Kiss, J, Murray, DW, Turner-Smith, AR, and Bulstrode, CJ: Roentgen Stereophotogrammetric analysis for assessing migration of total hip replacement femoral components. Proceedings of the Institution of Mechanical Engineers, Part H 209:169, 1995.

Ryd, L and Toksvig-Larsen, S: Early Postoperative Fixation of Tibial Components: An In Vivo Roentgen Stereophotogrammetric Analysis. Journal of Orthopaedic Research 11:142, 1993.

Santos-Munne, JJ. Stereotactic System for Linear-Trajectory Medical Interventions. 5-13-1996. Northwestern University. Thesis/Dissertation

Selvik, G: Roentgen stereophotogrammetry. A method for the study of the kinematics of the skeletal system. Acta Orthop.Scand.Suppl. 232:1, 1989.

Wang, S, Jones, NB, Richardson, JB, and Klaassens, E: Optimised method for locating reference markers in roentgen stereophotogrammetric analysis of orthopaedic radiographs. Medical and Biological Engineering and Computing 34:88, 1996.

Appendix D - Control Hardware Details

Hardware Details

1.0 Introduction

While the theory of minimally constrained cobots is useful in understanding the behaviour and control laws, a physical control architecture is also necessary to build a prototype. The framework for controlling a four legged parallel cobot has been implemented. This includes design, selection of components, purchase and installation into a prototype 'black box'. The main goal of the system is to control 4 steering motors that are part of the CVTs for each leg of the platform.

Real time control is achieved through the use of Matlab's "Real Time Workshop" (RTW). Run on a PC, RTW is capable of position control on the motors by running a customized PID controller. RTW communicates with the motors through Humusoft's MF 604 board, which has 4 channels of D/A, 4 channels of optical encoder feedback, and various DIO capabilities. A digital voltage is generated by the position controller and sent to the D/A port of the MF 604. This signal is converted into an analog voltage, which is amplified by a set of Maxon's "Linear Servo Controllers". Power for amplification is supplied by a 4.8 ampere power supply. The amplified control voltage drives the motors directly.

The control loop is closed by optical encoder feedback from the motors. The motors have a 100 counts/turn optical encoder on the end of a 19:1 planetary gearhead. The result is a feedback resolution of 1900 counts/turn. This information passes straight to the Humusoft board, which updates a register with the current position information.

As mentioned, a low level position controller was programmed for the motors. Initial tests confirm that the program works, however optimization of the controller variables are necessary for operation. Substantial time was invested in further controller development, but was limited by bugs in third party software.

The rest of this Appendix describes the hardware and how it is used in the prototype of a minimally constrained parallel cobot. Not all technical information is included, however, a hard copy of documentation for any piece of hardware can be found in the Neuromotor Control Lab. Supplier contact information is located at http://ncl.mech.ubc.ca/supplier.htm.

2.0 List of Major Hardware:

2.1 Motors

We are using Maxon's A-max 3.5 precious brush motors (# 110137), in conjunction with a 19:1 planetary gearhead (#110356), and a 100 count per turn digital encoder (#110520). Four of these motors are used to drive leg links around the CVT mechanism.

2.2 Linear Amplifiers

The linear amplifiers we use take an input voltage and try to perform velocity control on the motors. We use Maxon's Linear Servo Controller. This servo controller takes a +/- 10 V input.

2.3 I/O Board

The I/O board that allows encoder feedback from the motors and D/A for the linear servo controllers is Humusoft's MF604. The D/A is fixed to +/- 10V and it has 4 channels D/A and encoder support.

2.4 Power Supply

Maxon's LSCs require power to amplify the input signal, and this is supplied by an open case AC/DC converter (Tectrol GHOF 3 Series). The converter supplies 24V at up to 4.8 A.

2.5 Voltage Limiter

The computer fan requires a 12 V input. The 24V power supply is managed by using a Motorola MC 7800 voltage limiter. It is mounted on the side of the power supply and has a heat sink attached.

2.6 Wiring

All wiring is made by Allied Custom Cable. The wiring going to the motors is oil and water proof, 3 conductor, 18 gauge wire. There is a 30 foot, 37 conductor, female to open wire for the encoder feedback, and a 6 foot, 37 conductor, male to female cable for the control voltages for the motors.

3.0 Overall Setup

The computer containing the Humusoft MF 604 card has 2 - 37 pin female D-sub connectors. The first one contains the D/A signals and the second contains the interface to the motor encoders.

The output voltages are sent to a modified 386 case (power case) which contains the amplifiers and power supplies for the motors. The signals come into the power case through a 37 pin male connector. Connections to the motors are made through 4 banana plugs to the back of the case. They are labeled 1 to 4 from top to bottom. Power for the device is supplied through the normal AC computer plug. Connecting the AC plug will provide power to all the components immediately, since there is no off/on switch. The power supply is protected with an inlined fuse on the live AC wire. There are extra fuses available in the lab if needed and they are specified in the documentation for the power supply.

The encoders signals arrive over a 37 conductor open - male plug straight from the remote manipulator to the computer I/O board.

Appendix E – Calling Convention for MATLAB Simulation

ORGANIZATION OF SIMULATION

Organization of of Cart Simulation Matlab Files

Function go_rich.m

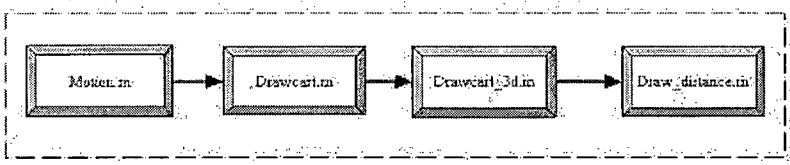

go_rich.m orchestrates the simulation by solving for the cart configuration at each time step. It also calls all graphing programs.

Function motion.m

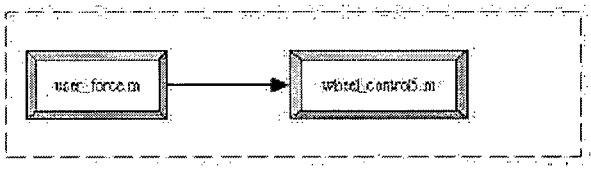

Matlab uses an ode solver on motion.m to determine the new state variables for the cart

Function wheel_control5.m

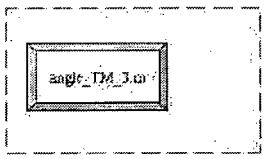

Matlab optimizes the wheel angle at that time step through 'angle_TM_3.m' and returns it to wheel_control5.m which then uses a PD controller to determine steering wheel velocity

DESCRIPTION OF FUNCTIONS

Matlab Function	Description
Motion.m	• Parent program for simulation • Contains all major variables, such as PD controller variables, cart description and initial conditions for the simulation • Uses ode solver to call subfunction motion.m to solve for configuration at each time step • Creates all figures after simulation is complete
Drawcart.m	• Draws a topographical depiction of the cart moving in a plane
Drawcart_3d.m	• Draws a 3D plot containing points of the cart configuration at each time frame • Graphs a plane representing the TM (This feature is hardcoded and much be changed manually)
Draw_distance.m	• Draws a 2D plot of the perpendicular distance from the Target Manifold
User_force.m	• Determines the forces applied at each time step • Uses the virtual trajectory description, which has a predetermined motion of the users hand, and then constructs the forces by attaching a spring between the actual configuration and the virtual trajectory of the user's hand motion
Wheel_control5.m	• This function is responsible for controlling the velocity of the wheel • Used to control the steering motors via a PD controller • Optimizes subfunction angle_TM_3 for ideal wheel direction
Angle_TM_3.m	• Cost function based on wheel orientation, and cart configuration • Used to determine correct change in wheel orientation to obtain correct heading angle with the target manifold

Appendix F - CVT Component Drawings

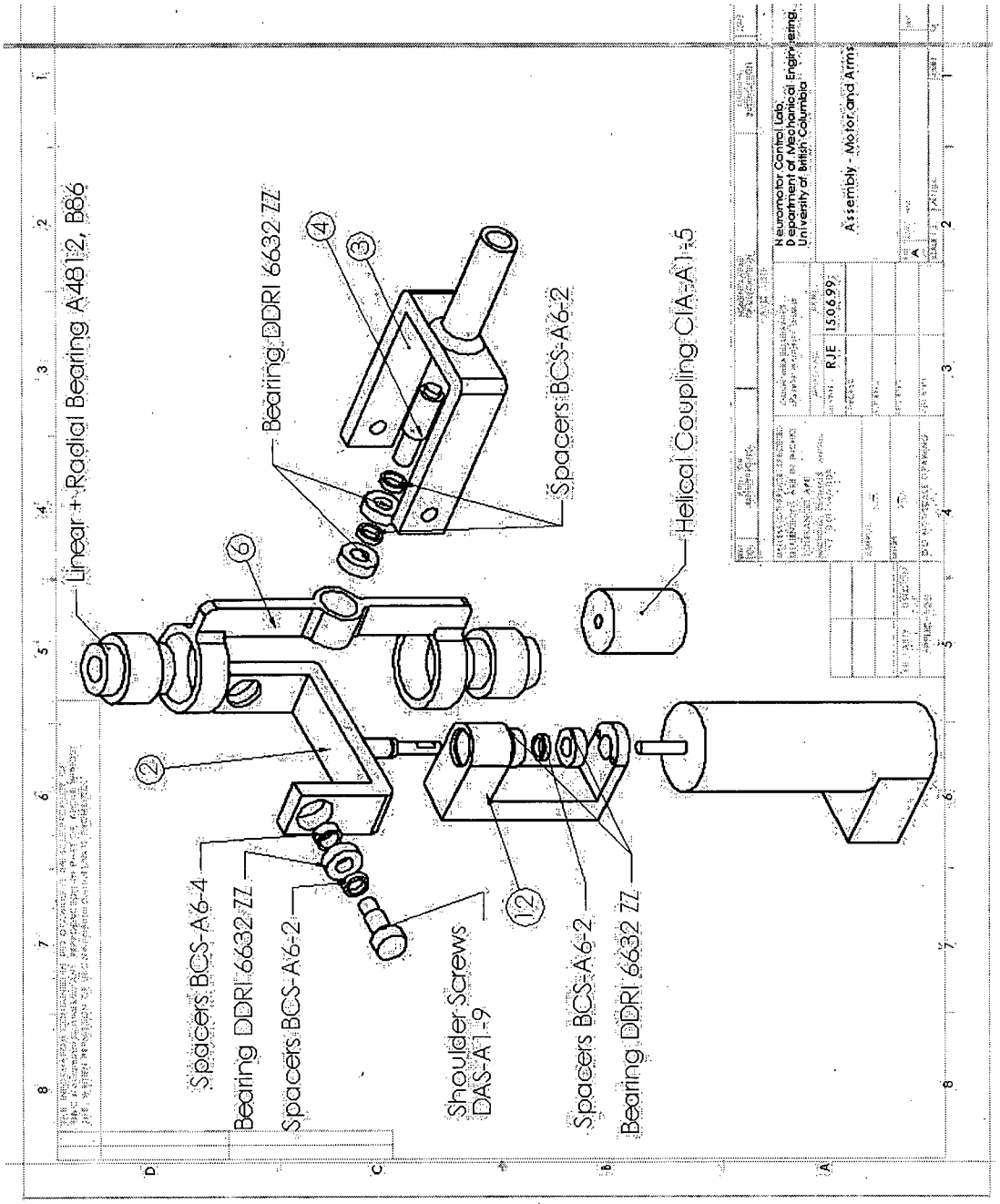
Linear + Radial Bearing A481-2, B86
Bearing DDRI 6632 ZZ
Spacers BCS-A6-2
Helical Coupling CIA-A1-5
Spacers BCS-A6-4
Bearing DDRI 6632 ZZ
Spacers BCS-A6-2
Shoulder Screws DAS-A1-9
Spacers BCS-A6-2
Bearing DDRI 6632 ZZ
Neuromotor Control Lab.
Department of Mechanical Engineering.
University of British Columbia
Assembly - Motor and Arms
RJE
1506.99

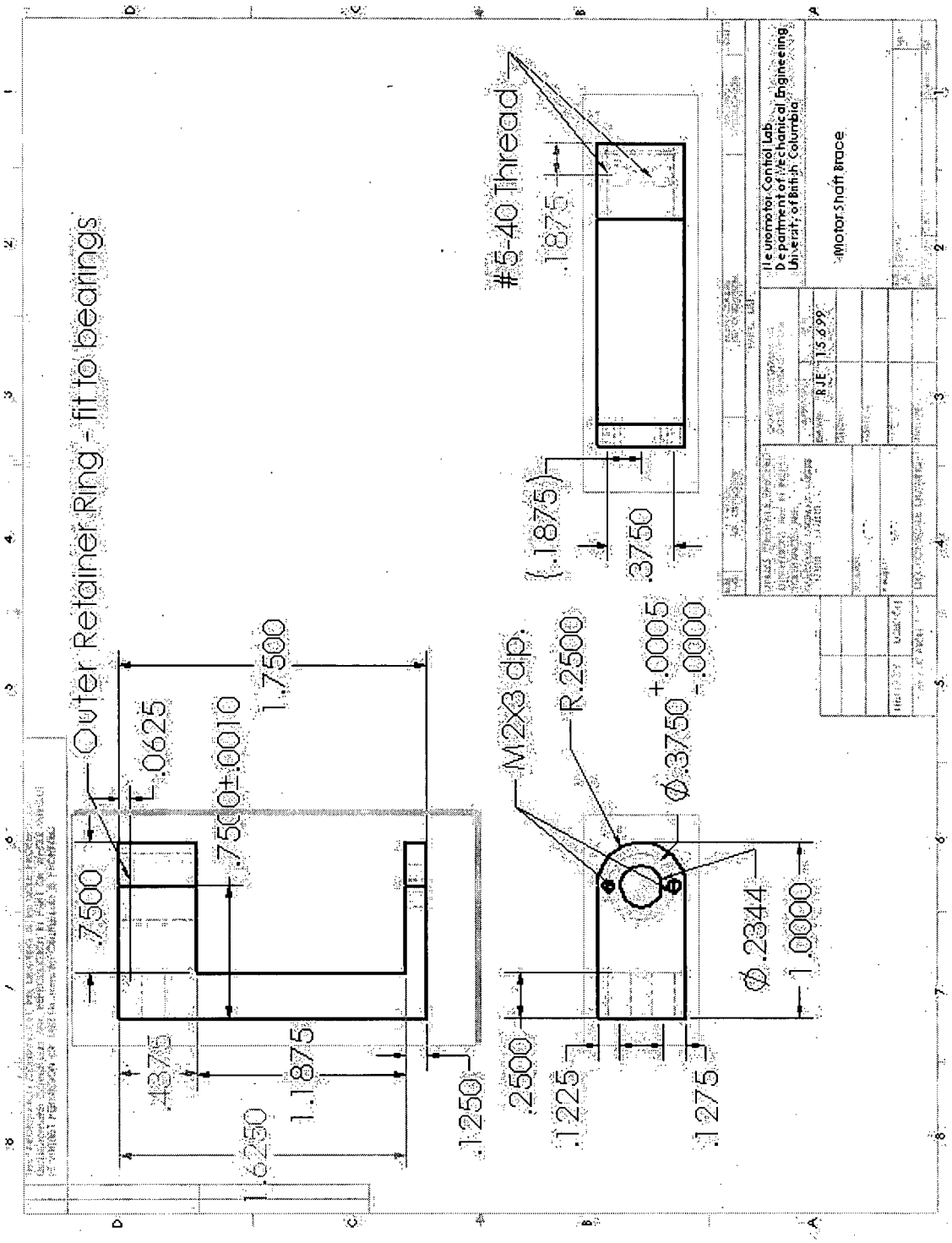
Outer Retainer Ring - fit to bearings
.7500
.0625
1.7500
.7500±.0010
.4375
1.1875
1.6250
.1250
M2X3 dp.
R.2500
Ø.3750 +.0005 -.0000
Ø.2344
1.0000
.2500
.1225
.1275
#5-40 Thread
.1875
(.1875)
.3750
Motor Shaft Brace
B.J.E. 15 ø99

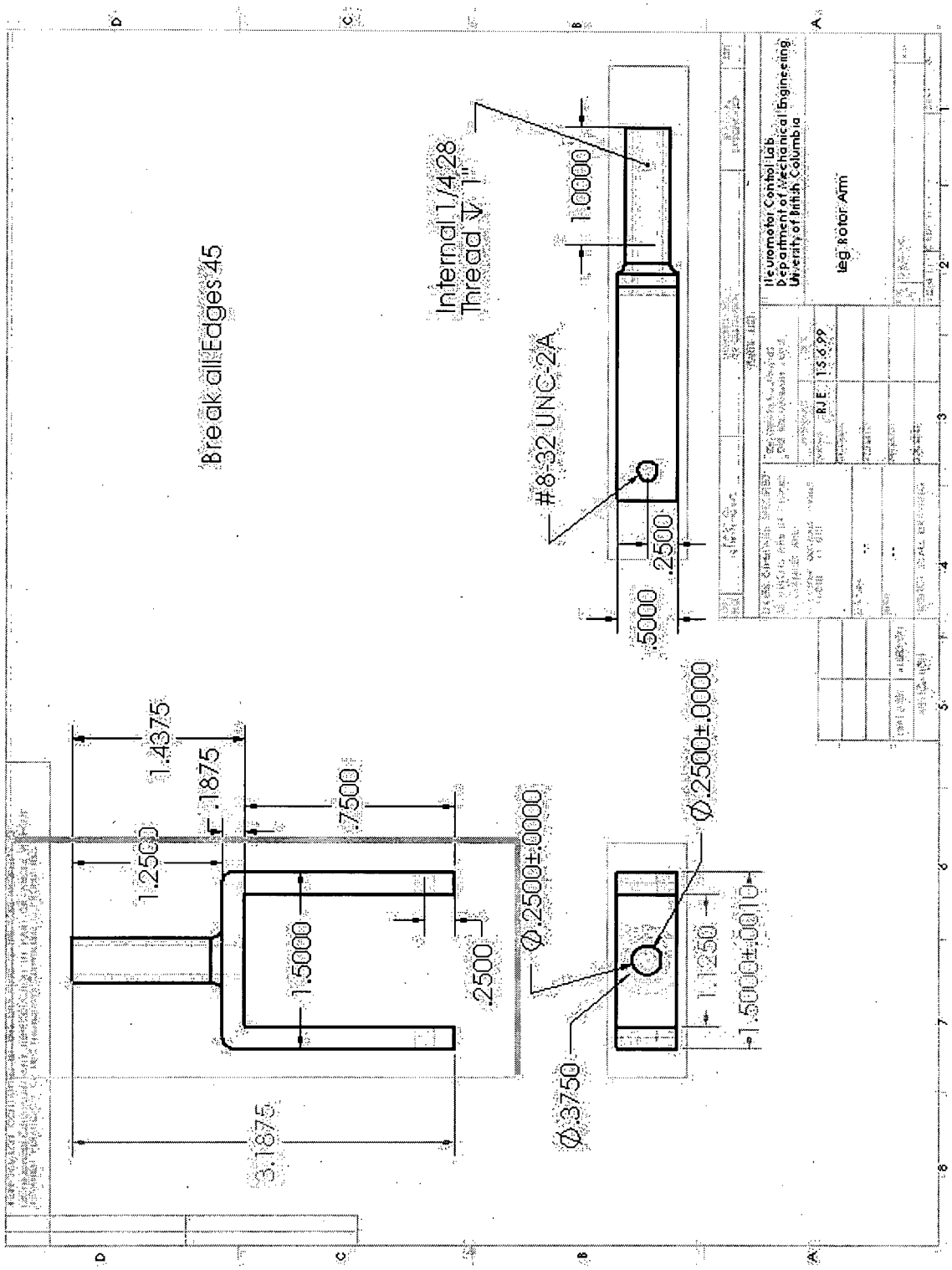
Break all Edges 45
Internal 1/4-28
Thread ↧ 1"
1.0000
#8-32 UNC-2A
.2500
.5000
1.4375
.1875
.7500
1.2500
1.5000
.2500
Ø.2500±.0000
Ø.2500±.0000
1.1250
1.5000±.0010
Ø.3750
3.1875
Pneumatic Control Lab
Department of Mechanical Engineering
University of British Columbia
leg Rotor Arm
RJE 13.6.99

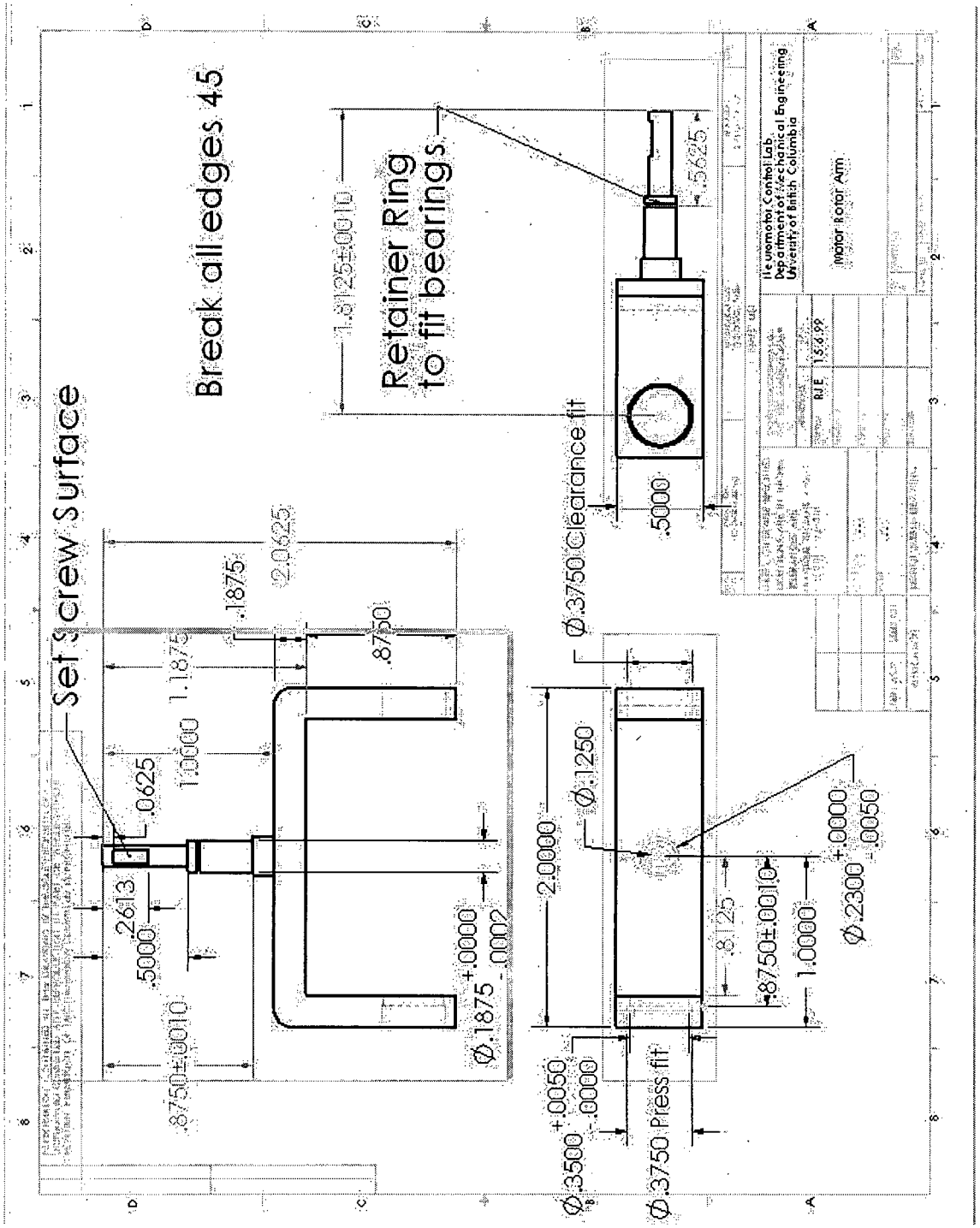
Set Screw Surface
Break all edges 45
Retainer Ring
to fit bearings
1.8125±.0010
.5625
.5000
Ø.3750 Clearance fit
2.0625
.1875
.8750
1.1875
1.0000
.0625
.2613
.5000
.8750±.0010
Ø.1875 +.0000 -.0002
Ø.1250
2.0000
.8125
.8750±.0010
1.0000
Ø.2300 +.0000 -.0050
Ø.3500 +.0050 -.0000
Ø.3750 Press fit
Motor Rotor Arm
Department of Mechanical Engineering
University of British Columbia

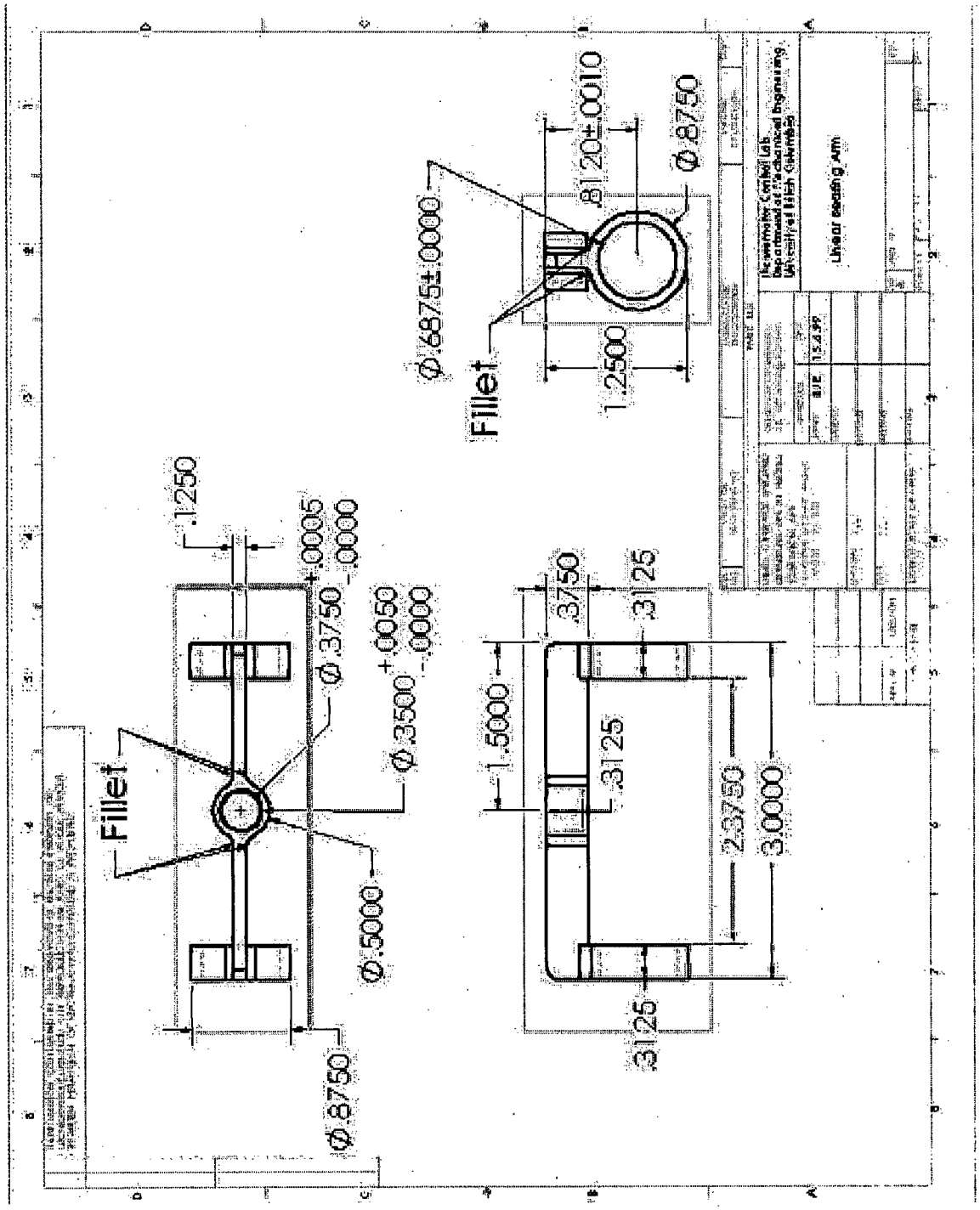
Fillet
.1250
Ø.3750 +.0005 -.0000
Ø.3500 +.0050 -.0000
Ø.5000
Ø.8750
Fillet
Ø.6875±.0000
.8120±.0010
Ø.8750
1.2500
.3750
.3125
1.5000
.3125
2.3750
3.0000
.3125
Linear Reading Arm